TRACTION MODELING AND CONTROL OF A DIFFERENTIAL DRIVE MOBILE ROBOT TO AVOID WHEEL SLIP

By

EDISON ORLANDO COBOS TORRES

Bachelor of Science in Mechanical Engineering
Escuela Politécnica Nacional
Quito, Ecuador
2007

Submitted to the Faculty of the
Graduate College of
Oklahoma State University
in partial fulfillment of
the requirements for
the Degree of
MASTER OF SCIENCE
December, 2013

TRACTION MODELING AND CONTROL OF A DIFFERENTIAL DRIVE MOBILE ROBOT TO AVOID WHEEL SLIP

Thesis Approved:

Dr. Prabhakar Pagilla

Thesis Advisor

Dr. Don Lucca

Dr. Girish Chowdhary

ACKNOWLEDGMENTS

I would like to thank to God for give me all the necessary strength to accomplish this.

I would like to thank to Dr. Pagilla for giving the opportunity to work with him in the laboratory, for his advise to improve my knowledge and face the problem of slippage and others with useful tools, and for his wisdom and kindness. For these reasons and others, I would like to extend to him my admiration.

I would like to thank Dr. Don Lucca and Dr. Girish Chowdhary for being part of my thesis committee, their comments, and their patience.

I would like to thank to Fulbright and Fulbright-Ecuador for believing in me, and always being there for any reason with their support and friendship.

I would like to express my consideration and friendship to Shyamprasad Konduri, who guided me until this point. As well, Emilio Gabino, Venkata Gidda, and Andrew Burnap for their collaboration in the project and for being not only colleagues but also friends.

I dedicate this work to my son for being my inspiration and reason to live, to my wife for her support, and to my parents.

Acknowledgements reflect the views of the author and are not endorsed by committee members or Oklahoma State University

Name: Edison Orlando Cobos Torres

Date of Degree: December, 2013

Title of Study: TRACTION MODELING AND CONTROL OF A DIFFERENTIAL DRIVE MOBILE ROBOT TO AVOID WHEEL SLIP

Major Field: Mechanical and Aerospace Engineering

Scope and Method: The motion of a differential drive mobile robot with consideration of slip at contact between the wheels and the ground is studied in this work. Traction forces between the wheel and the ground are derived by considering a rigid wheel, rigid ground interaction model and a caster wheel which provides support to the mobile robot during motion. The motion governing equations are determined by incorporating the traction forces. Numerical simulations are conducted to learn the motion behavior of the robot with wheel slip for a range of wheel input torques. Based on the traction force model and observations from numerical simulations, a slip avoidance controller that limits the input torques is developed. Experiments are conducted to verify the characteristics of the dynamic model with slip and the control strategy used to avoid slip.

Findings and Conclusions: Models that describe the dynamics of a differential drive mobile robot with and without slip are presented and discussed. A traction force model is developed by considering a simple Coulomb friction model. The caster wheel plays an important role in determining the traction forces. The longitudinal and lateral velocities of the wheel are used to compute the longitudinal and lateral forces. Wheel slip occurs if the reaction force exerted by the applied torque is greater than the static frictional force, which is calculated by the proposed model and this limit is used to implement a slip avoidance controller. Numerical simulations and experiments of the system using the proposed traction model reveal that the angular velocity of the wheels is greater than the corresponding linear velocity when slip occurs. The proposed torque limiting controller to avoid slip is also implemented in numerical simulations and experiments. Experimental results show a good correlation with the numerical simulations, thus verifying the approach and the developed dynamic model with wheel slip.

ADVISOR'S APPROVAL: Dr.Prabhakar Pagilla

TABLE OF CONTENTS

LIST OF TABLES

Table Page

LIST OF FIGURES

CHAPTER I

INTRODUCTION

Research related to design, modeling and control of mobile robots has been one of the most active areas of robotics in the last few decades. The use of mobile robots in various areas of human life has been continuously increasing. Mobile robots are being used as autonomous cleaning devices at homes, for factory automation, to patrol national borders, for bomb disposals, for hazardous waste cleaning, etc. One of the goals of research in mobile robotics is to make the mobile robots completely autonomous, that is, the robots are capable of making decisions based on sensing the environment they are in. Another area where mobile robots are employed is in cooperative control of multiple mobile robots which has received considerable attention in the last two decades with application in distributed transportation, monitoring and multi-point surveillance.

Mobile robots may be imparted motion using legs, spasmodic movements, or wheels. Wheeled mobile robots are common and typically consist of a combination of driven wheels and steering wheels or differential drive wheels. A differential drive robot is a type of wheeled mobile robot which comprises of two independent driven wheels to achieve linear and angular position and one (or several) caster wheel(s) to provide balance. A differential drive mobile robot is one of the simplest type of wheeled mobile robot which is easy to assemble and can be used for a wide variety of applications. It is constructed using the most basic of the wheel configurations. Since it consists of two driven wheels and no steering wheels, the robot is

steered using a difference in velocity between the two driven wheels; hence the name "differential drive robot." For these reasons it is one of the most used configurations in laboratories and real applications. A picture of a differential drive mobile robot is shown in Figure I.1.

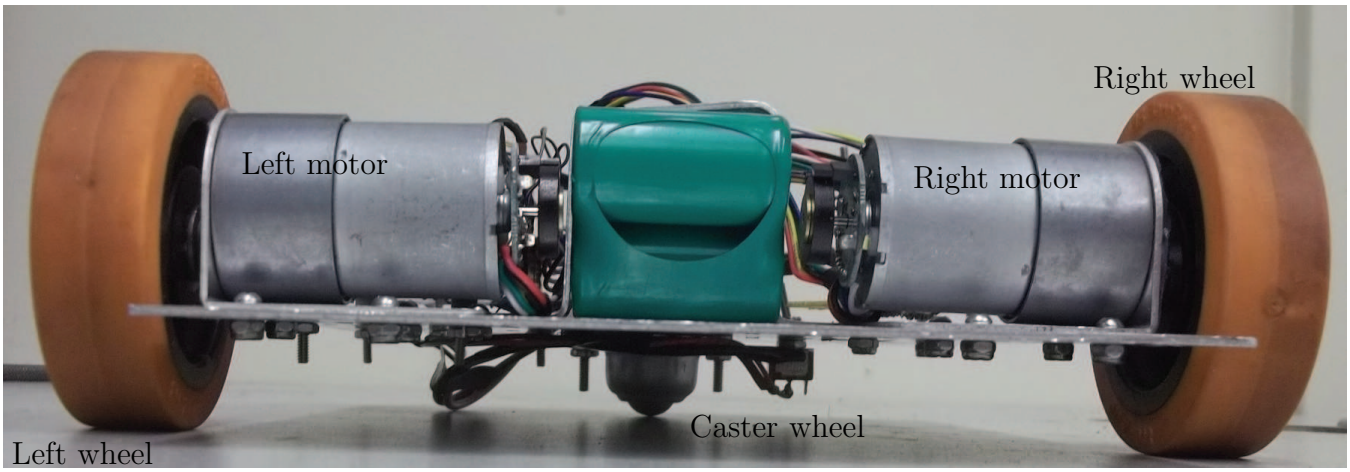

Figure I.1: Differential Drive Robot

There have been number of studies on the design, dynamic modeling and control of wheeled mobile robots, including differential drive robots. Most of the research in differential drive robots has assumed pure rolling conditions, that is all the torque provided to the robot wheels is used to generate motion of the robot without any losses due to slippage between the wheels and the surface on which the robot is moving. However, in practice the pure rolling assumption does not always hold. The robot wheels slip depending on wheel accelerations and traction forces between the wheels and the ground. The possibility of wheels slipping is higher in differential drive robots as the velocity differential between the two wheels is employed to generate turning or angular motion of the mobile robot. In an effort to mitigate wheel slip, it is beneficial to predict when slip occurs as a function of the applied torque to the wheels; this will help in accurately controlling of the position of the robot.

I.1 Mobile Robot Research under Pure Rolling Condition

There is a considerable amount of literature on differential drive robots, especially under the pure rolling assumption. Kinematics and dynamics of a number of the wheeled mobile robots have been developed and controllers were designed for achieving various motion control objectives, for details refer to [1–5]. A stable nonlinear path controller for the differential drive robot is developed in [1]. In [2,6] the nonlinear dynamics of the differential drive robot are linearized using input-output linearization. The internal dynamics of the robot system are derived by taking the output to be a look ahead point which is any point on the longitudinal axis of the robot other than on the wheel axle. It is reported that the system is asymptotically stable when the robot moves forward, but unstable when it moves backward. A two layer controller was used for position tracking in [3]; the first layer stabilizes the kinematics using a nonlinear path controller from [1] and the second layer uses an acceleration control to stabilize the velocity of the robot. In [5], a platoon of differential drive robots are used to track a reference trajectory for the platoon where potential problems due to wheel slip are reported to cause tracking errors.

All the above mentioned papers assume the condition of pure rolling while modeling the dynamics of the robot. Many applications that involve tracking a desired trajectory or reaching a set point require the mobile robot to be able to accurately define its position and orientation during motion. Predicting the onset of slip and controlling applied torque on the wheels to avoid slip based on this prediction will significantly help in accurate position control of the robot.

I.2 Mobile Robot Research Assuming Slip

Slip is a common phenomenon in wheeled vehicles. For example, a car slips when driven over ice or water, making high velocity turns, or accelerating/decelerating rapidly. When the arc length traversed by the wheel due to its angular motion is greater than its linear displacement on the surface, then it is clear that slip has occurred, i.e., the wheel rotates but does not have a corresponding angular motion. A similar effect calls skid is when the wheel has linear motion but does not have a corresponding angular motion. Slip may occur in the longitudinal direction or the lateral direction of wheel motion as shown in Figure I.2 where the longitudinal slip is produced as a result of a rapid acceleration on a hill and the lateral slip occurs when making a high velocity turn on a wet road. When both longitudinal and lateral slip occur simultaneously, the angle between the lateral and longitudinal motion directions is called the slip angle. To understand slip one has to study the interaction between the

Figure I.2: Longitudinal [7] and lateral slip [8]

ground and the wheels. Some definitions such as longitudinal slip, lateral slip and slip angle are introduced to describe slip.

The area in which interaction between rigid wheels on soft surfaces or soft wheels on hard surfaces is referred to as "terramechanics." This interaction could be complex based on the level of detail that is considered and there are several theories and approximations, to rep-

resent and describe this phenomenon. Models based on these theories, its approximations and traction experiments are described in [9] and its references. However, in all the studies the properties of the tire and ground play an important role in the determination of the coefficient of friction and traction forces. Although these models provide considerable understanding of the characteristics of the wheels and the ground, they require a number of parameters that characterize the wheels and ground to obtain the evolution of slip during motion.

A number of advances has been made towards predicting and controlling the behavior of the robot when it slips. In [10] equations of a mobile robot with slip are given along with a formulation of the adhesion coefficient for an omnidirectional wheel. It is stated that slip can significantly affect the position of the robot. A model for a flexible wheel that describes ground-wheel interaction is used in [11]; it is reported that this model can predict the position errors due to wheel slip for flexible wheels. Results from terramechanics have been used in robotics to study wheel slip in relevant cases [12–15]. The interaction between a rigid wheel and loose soil is considered in [12] and the relationship between the lateral traction force on the wheel and the slip angle is experimentally verified. The ability of a wheeled robot to climb on a rough terrain is improved by limiting wheel slip [13]; this work considered only longitudinal motion. A robot with four wheels on sand is considered in [16], where the intent was to track any path with different curvatures. Through the use of model simulations it is reported that limiting the torque applied to the wheels can minimize slip and achieve better tracking results. In [14] an image processing technique is used to compare the environment of the robot with known terrains, so a similar value of slip is assigned to the actual terrain. This technique is used to avoid slip in unknown environments. In [17] the dynamics of the robot under slip are introduced and for designing the controller only lateral slip is considered; the controller that is developed is based on a "look ahead point" with the desired trajectory

for this point being straight and curvilinear. In [18], Newton's equations are used to develop the mobile robot dynamic model, and both lateral and longitudinal slip are considered; a discontinuous feedback control law is used for robot motion stabilization. All the above mentioned work is based on terramechanics and the analysis is primarily directed towards interaction between soft wheels and rigid ground.

Some literature in the last decade focused on rigid wheel and rigid ground interaction and the wheel slip associated with it. In [19], a relationship between the traction forces and applied wheel torques is obtained. A controller with two levels is considered, where the first level deals with robot and wheel motor dynamics and the second level deals with the changes in the environment in which the robot operates in order to track a desired trajectory; it is indicated that the measurement of the global location of the robot is necessary to effectively control the robot and to determine if the robot slips. In [20], a traction force model with static friction between wheel and ground is considered; the effect of the caster wheel on the traction forces is ignored. Depending on the magnitude of the traction forces, the evolution of robot motion is obtained by switching the models that consider slip and pure rolling conditions. None of the literature reviewed on rigid wheel rigid ground interaction has experimentally verified the proposed models.

In this work, rigid wheel, rigid ground interactions are considered. Traction forces are modeled considering both static and kinetic coefficients of friction. The effect of caster wheel on calculating the normal forces is included in the dynamic model. The presence of the castor wheels affects the slip behavior of the mobile robot.

I.3 Contributions

The contributions of this work are summarized below:

- A dynamic model for a differential drive robot is developed by considering rigid wheel, rigid ground interaction, static and kinetic friction, and the effect of the caster wheel. The model is used to predict the maximum torque that can be applied to the wheel before it starts to slip. Model simulations were conducted to study the motion behavior of the robot under pure rolling and slip conditions.

- A control strategy that can be employed to avoid wheel slip by limiting the applied wheel torque is proposed. The maximum permissible torque for a given surface, which is the value of the torque at which the wheel slips, is used to limit the applied wheel torque.

- Experiments were conducted using a differential drive robot to corroborate the models and the approach. The proposed controller is evaluated by conducting several mobile robot motion experiments.

The rest of this report is organized as follows. The dynamics of the differential drive robot under pure rolling and slip conditions are described in Chapter II. The traction forces that are used in studying slip, a controller to avoid slip, and model simulations are also given in this chapter. The mobile robot and associated hardware used in experiments are given in Chapter III. The results of the experiments on establishing the coefficients of friction, validating the traction force model, and the slip avoidance controller are presented in this chapter. Conclusions of this work and possible future work are presented in Chapter IV.

CHAPTER II

DYNAMICS OF A DIFFERENTIAL DRIVE WHEELED MOBILE ROBOT CONSIDERING SLIP AND TRACTION FORCES

There is an extensive amount of literature related to the development of dynamic models for wheeled mobile robots [1, 17, 18, 20–22]. Although the resulting models are different based on the construction of the robot, such as number and location of wheels, types of actuators, etc., the underlying principles that are employed to obtain the models are the same; either Euler-Lagrange equations or Newton's equations are typically used to obtain the dynamic equations that describe the motion of the robot.

The wheeled mobile robot is treated as a rigid body that translates and rotates in a plane. Therefore its coordinates of motion are given by position (x, y) in the plane and its orientation (ϕ). The differential drive wheeled mobile robot considered in this work consists of two wheels that are actuated with two independent motors and a free caster wheel that balances the robot platform during motion. The motors provide necessary input torques (τ_r, τ_l) which can be used to command the required motion for the robot. Since the angular speed of the wheels are regulated at the same value to obtain a straight line motion to the robot, orientation of the robot is obtained by a difference in the angular speeds of the two driven wheels.

In this chapter, we first describe the kinematics and dynamics of the differential drive robot

under pure rolling conditions and without lateral wheel slip. Then the pure rolling and lateral motion constraints are relaxed to obtain a complete model that includes both lateral and longitudinal slip. A wheel-ground friction model that can be used to obtain reaction forces between the wheels (both driven and castor) and the ground is developed. These reaction forces are used to estimate the slip between the wheels and the ground. A strategy to control the robot to follow a desired trajectory is given to avoid slip during motion of the robot.

II.1 Differential Drive Odometry

The first step is to understand a differential drive mobile robot odometry and to review some helpful concepts [23]. The nomenclature that is used in this chapter is given in Table II.1.

Consider the rigid body shown in Figure II.1 that is translating and rotating in the plane.

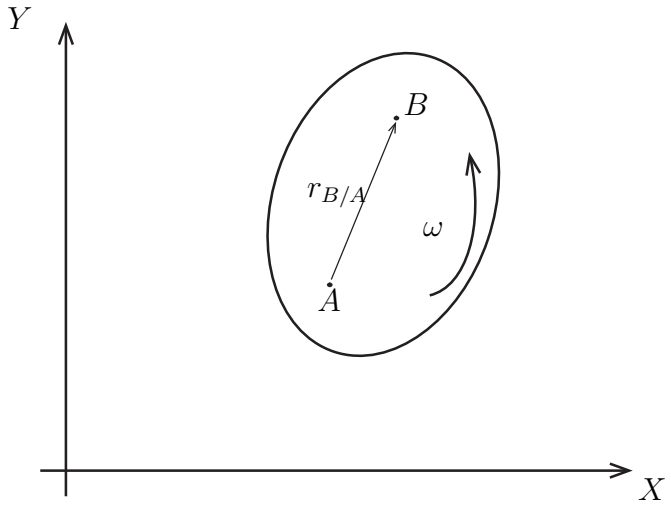

Figure II.1: Rigid body on the plane

Table II.1: Nomenclature

Variable	Symbol	Unit
Acceleration	a	m/s^2
Angular position of the robot	ϕ	rad
Angular speed of the wheels	$\dot{\theta}$	rad/s^2
Angular velocity of the robot	ω	rad/s
Coefficient of kinematic friction	μ_k	
Coefficient of static friction	μ_s	
Distance between wheels	$2b$	m
Distance from center of mass to caster wheel	e	m
Distance from wheel's axis to center of mass	d	m
Gravity acceleration	g	m/s
Height from floor to center of mass	h	m
Lateral forces	F_{lat}	N
Lateral velocity of the robot	$\dot{\eta}$	m/s
Linear velocity	V	m/s
Longitudinal forces	F_{long}	N
Longitudinal velocity of the wheel	$\dot{\rho}$	m/s
Main axis	$OXYZ$	
Mass of robot platform	m_r	kg
Normal forces	N	N
Robot axis	$oxyz$	
Robot moment of inertia about the vertical axis	I_{rz}	kg m^2
Torques	τ	m-N
Total inertia	I_t	kg m^2
Total mass	m_t	kg
Wheel mass	m_w	kg
Wheel moment of inertia about the vertical axis	I_{wz}	kg m^2
Wheel moment of inertia about the wheel axis	I_{wy}	kg m^2
Wheel radius	r	m
Subscripts		
r: pertaining to the right wheel l: pertaining to the left wheel L: pertaining to the linear motion A: pertaining to the angular motion		

The relative velocity between two different points in the rigid body is given by

$$V_B = V_A + \omega \times r_{B/A} \tag{II.1}$$

where V_A is the velocity of point A, V_B is the velocity of point B, ω is the angular velocity of the body, and $r_{B/A}$ is the position vector directed from A to B. From this equation, we can observe that when the body does not have any angular velocity, all the points in the body will have the same linear velocity. Taking the time derivative of Equation (II.1) the following relationship for acceleration is obtained

$$a_B = a_A + \alpha \times r_{B/A} - (\omega)^2 \times r_{B/A} \tag{II.2}$$

where a is the acceleration of the respective point and α is the angular acceleration of the body. Our rigid body is the differential drive robot shown in II.2, where the position of components is determined by the direction of the motion and the position of the caster wheel.

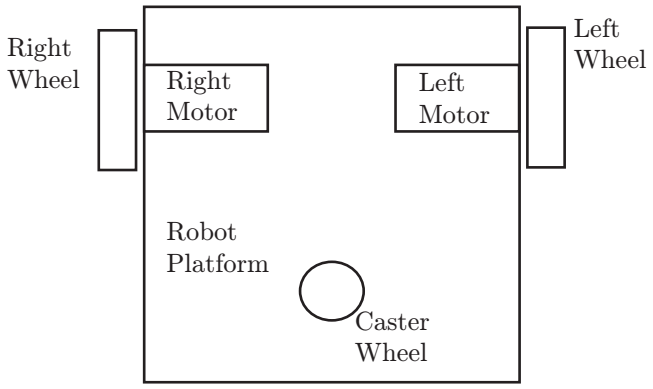

Figure II.2: Robot configuration

The above equations can be used to know the velocity and acceleration of any point in the robot when it moves in the plane and these equations will be used later in the chapter in

the derivation of the dynamics of the mobile robot.

II.2 Differential Drive Robot under Pure Rolling

II.2.1 Mobile Robot Kinematics

To derive the kinematics of the robot, consider a simple illustration of mobile robot as shown in Figure II.3. The position and orientation of the robot at any instant of time are described by the vector $q = [x, y, \phi]^T$, where (x, y) denote the position of point o (the center of the axis of the driven wheels) and ϕ is the orientation of the robot in the global coordinate frame. The angular velocity of the left and right wheels are denoted by $\dot{\theta}_l$ and $\dot{\theta}_r$, respectively. There

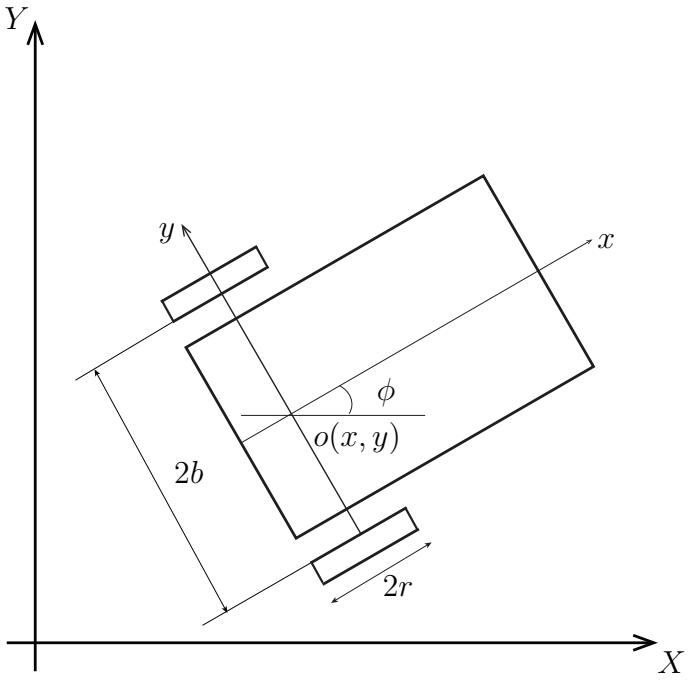

Figure II.3: Two Wheeled Differential Drive Robot [5]

are three variables to control (x, y, ϕ) and only two control inputs (wheel torques), therefore, the system is under-actuated. The relationship between the linear velocity v and the angular

velocity ω of the robot and the rate of change of position and orientation is given by

$$\begin{bmatrix} \dot{x} \\ \dot{y} \\ \dot{\phi} \end{bmatrix} = \begin{bmatrix} \cos\phi & 0 \\ \sin\phi & 0 \\ 0 & 1 \end{bmatrix} \begin{bmatrix} v \\ \omega \end{bmatrix} \tag{II.3}$$

The above equation represents the kinematics of the robot. It is noted that the geometric center of the robot need not be the center of mass of the robot. The center of wheel rotation axis (point o) is taken as the reference point of rotation. Hence, the velocity at this point o is taken as the velocity of the robot. The rotation angle is not restricted to the robot's reference frame, because as a rigid body all points undergo the same change in orientation. When $\dot{\theta}_r$ is greater that $\dot{\theta}_l$, then the robot turns to the left of its current position and the orientation angle increases and if $\dot{\theta}_l$ is greater than $\dot{\theta}_r$ the robot turns right. The linear and angular velocities of the robot may be related to the wheel angular speeds by

$$v = \frac{r(\dot{\theta}_r + \dot{\theta}_l)}{2} \tag{II.4}$$

$$\omega = \frac{r(\dot{\theta}_r - \dot{\theta}_l)}{2b} \tag{II.5}$$

where r is the radius of the wheel and $2b$ is the length of the wheel base, that is, the distance between the wheels measured along the rotation axis of the wheels. Although it is not used in designing a kinematic controller, it is worthy to note an important constraint on the robot's motion. This constraint is non-holonomic and restricts lateral slip of the wheels, thus restricting any lateral motion. It is given by the following equation:

$$\dot{x}\sin\phi = \dot{y}\cos\phi \tag{II.6}$$

Solving the above equations and considering the non-holonomic constraints, it is possible to obtain the following equations:

$$\dot{\theta}_r r = \dot{x}\cos\phi + \dot{y}\sin\phi, \tag{II.7}$$

$$\dot{\theta}_l r = \dot{x}\cos\phi + \dot{y}\sin\phi \tag{II.8}$$

These are common relationships, and it is possible to express them as a function of the center of the mass (c) of the robot using Equations (II.1) and (II.2) to relate these points. For this reason we will refer with subscript "o" when using the center of the wheels axis and with subscript "c" when we refer to the center of the mass.

II.2.2 Mobile Robot Dynamics

To obtain the dynamic equations of the mobile robot, we use the Lagrangian formulation. Since the mobile robot is on the ground which is taken as the datum, the Lagrange function is the total kinetic energy of the system and is given by

$$L = \frac{1}{2}m(\dot{x_o}^2 + \dot{y_o}^2) + \frac{1}{2}I_t\dot{\phi}^2 \tag{II.9}$$

The mobile robot dynamic equations are given by

$$\frac{d}{dt}\frac{\partial L}{\partial \dot{q_o}} - \frac{\partial L}{\partial q_o} = J^T(q_o)\lambda + B(q_o)\tau \tag{II.10}$$

where q_o is the generalized coordinate vector, i.e, $q_o = [x_o, y_o, \phi]^T$, $J(q_o)$ is the non-holonomic constraint matrix, λ is the Lagrange multiplier vector of constraint forces, $B(q_o)$ is the input transformation matrix obtained from the kinematics of the robot, and τ is the input torque

vector. Substituting the Lagrangian and using Equations (II.3), (II.9) in Equation (II.10), we obtain the robot dynamics as

$$\begin{bmatrix} m_t & 0 & 0 \\ 0 & m_t & 0 \\ 0 & 0 & I_t \end{bmatrix} \begin{bmatrix} \ddot{x_o} \\ \ddot{y_o} \\ \ddot{\phi} \end{bmatrix} = \frac{1}{r} \begin{bmatrix} \cos\phi & \cos\phi \\ \sin\phi & \sin\phi \\ b & -b \end{bmatrix} \begin{bmatrix} \tau_l \\ \tau_r \end{bmatrix} + \begin{bmatrix} \sin\phi \\ -\cos\phi \\ 0 \end{bmatrix} \lambda \tag{II.11}$$

where m_t is the mass and I_t is the inertia of the robot about its rotational axis. There are several methods to eliminate the Lagrangian multiplier λ. One can use the robot kinematics to get the accelerations and substitute the accelerations in the above equation. Another method is to use Boltzmann - Hamel equations [4]. The kinematics based method is employed in this work since the equations are relatively simple. The total applied torque is the sum of linear (τ_L) and angular (τ_A) torques. The linear and angular torques are given by

$$\tau_L = \frac{1}{r}(\tau_l + \tau_r), \quad \tau_A = \frac{2b}{r}(\tau_l - \tau_r) \tag{II.12}$$

where τ_l and τ_r are the torques provided by left and right motor, respectively. Using the linear and angular torques, Equation (II.11) can be written as

$$\begin{aligned} \ddot{x}_o =& \frac{1}{m_t}(\tau_L \cos\phi + \lambda \sin\phi) \\ \ddot{y}_o =& \frac{1}{m_t}(\tau_L \sin\phi - \lambda \cos\phi) \\ \ddot{\phi}_i =& \tau_A / I_t \end{aligned} \tag{II.13}$$

Differentiating the robot kinematics from Equation (II.3), substituting the vector $[\ddot{x}_o, \ddot{y}_o, \ddot{\phi}]^T$ in Equation (II.13) and solving for $[\dot{v}, \dot{\omega}]^T$ we obtain

$$\begin{bmatrix} \dot{v} \\ \dot{\omega} \end{bmatrix} = \begin{bmatrix} \tau_L/m_t \\ \tau_A/I_t \end{bmatrix} \tag{II.14}$$

Equation (II.14) is the dynamic equation of the robot referred to the center of rotation. These dynamics are used in designing a torque based motor controller for commanding the motion of the robot. Using the transformations given by Equation (II.2) and the dynamics of the wheels we obtain the following equations by considering the position of the center of mass:

$$M\ddot{q} = B\tau - C\lambda \tag{II.15}$$

where

$$M = \begin{bmatrix} m_t & 0 & dm_t \sin\phi & 0 & 0 \\ 0 & m_t & -dm_t \cos\phi & 0 & 0 \\ dm_t \sin\phi & -dm_t \sin\phi & I_t & 0 & 0 \\ 0 & 0 & 0 & I_{wy} & 0 \\ 0 & 0 & 0 & 0 & I_{wy} \end{bmatrix} \tag{II.16}$$

$$q = \begin{bmatrix} x_c \\ y_c \\ \phi \\ \theta_r \\ \theta_l \end{bmatrix} \quad B = \begin{bmatrix} \cos\phi/r & \cos\phi/r \\ \sin\phi/r & \sin\phi/r \\ b/r & -b/r \\ 1 & 0 \\ 0 & 1 \end{bmatrix} \quad C = \begin{bmatrix} dm_t\dot{\phi}^2 \cos\phi \\ dm_t\dot{\phi}^2 \sin\phi \\ 0 \\ 0 \\ 0 \end{bmatrix} \tag{II.17}$$

and $\tau = [\tau_l, \tau_r]^T$.

II.3 Differential Drive Robot Under Slip

II.3.1 Mobile Robot Kinematics with Slip

In the previous section kinematics and dynamics under pure rolling and without lateral slip are derived. However, in practice, there is slip in both lateral and longitudinal directions. Lateral slip is present when the direction of the movement is different from wheel's plane of rotation, so the wheel must slip in order to reorient itself in the desired direction; see Figure II.4.

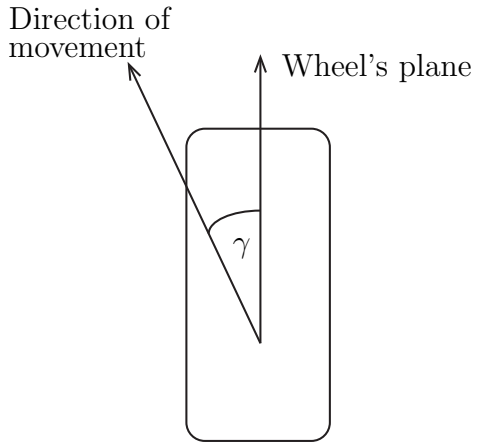

Figure II.4: Lateral slip due to difference in robot motion direction and plane of rotation of the wheel

Longitudinal slip occurs when the input torque is not completely transmitted to the ground. As a consequence, the linear speed of the wheel ($\dot{\rho}$) is not equal to the peripheral speed of the wheel, i.e., $\dot{\rho} < \dot{\theta} r$. A portion of the applied torque is transmitted to the ground resulting in wheel forward motion, the rest is consumed by pure wheel rotation causing wheel slip. Longitudinal slip is also possible when the wheel stops rotating but the linear velocity is not zero, this scenario is often referred to in the literature as skid. The focus of this work is on slip phenomenon, but a similar analysis may be applied when the robot skids.

Lateral slip is a phenomenon that has minimal affect on achieving a motion objective for the robot at low speeds. It can be observed mainly when the robot is in motion along a curved path at high speeds, i.e., when continuous and rapid orientation changes are required. Longitudinal slip is more prevalent as it is a direct consequence of the application of wheel torques beyond what can be supported by the traction between the wheels and the ground. It is directly influenced by the value of coefficient of friction along the motion path. In the following we provide equations of motion under slip.

In the presence of slip, the non-holonomic constraints are given by

$$\begin{aligned}
\dot{\rho_r} &= \dot{x_c}\cos\phi + \dot{y_c}\sin\phi + b\dot{\phi} \\
\dot{\rho_l} &= \dot{x_c}\cos\phi + \dot{y_c}\sin\phi - b\dot{\phi} \\
\dot{\eta} &= \dot{x_c}\sin\phi - \dot{y_c}\cos\phi - d\dot{\phi}
\end{aligned} \tag{II.18}$$

where $\dot{\eta}$ represents the lateral velocity due to slip and $\dot{\rho_r}, \dot{\rho_l}$ are the linear velocities of right and left wheels, respectively. Using the above equations, the kinematics of the differential drive robot can be expressed as

$$\begin{bmatrix} \dot{x_c} \\ \dot{y_c} \\ \dot{\phi} \end{bmatrix} = \begin{bmatrix} \cos(\phi) & -\sin\phi & -d\sin\phi \\ \sin(\phi) & \cos(\phi) & d\cos\phi \\ 0 & 0 & 1 \end{bmatrix} \begin{bmatrix} v \\ \dot{\eta} \\ \omega \end{bmatrix} \tag{II.19}$$

In the same manner, the kinematics of the robot can be related with the linear velocities of the wheel by

$$\begin{bmatrix} \dot{\eta} \\ v \\ \omega \end{bmatrix} = \begin{bmatrix} 1 & 0 & 0 \\ 0 & \frac{1}{2} & \frac{1}{2} \\ 0 & \frac{1}{2b} & \frac{1}{2b} \end{bmatrix} \begin{bmatrix} \dot{\eta} \\ \dot{\rho_r} \\ \dot{\rho_l} \end{bmatrix} \tag{II.20}$$

Using the given definitions, it is sometimes beneficial to define the total linear displacement of the wheel as:

$$\rho = \theta r - \delta \tag{II.21}$$

where θr is the arc length traversed and δ represents the loss of displacement due to slip.

II.3.2 Mobile Robot Dynamics with Slip

Under wheel slip, because the applied torque is not fully transmitted to the ground, to derive dynamic equations, one must consider the required forces involved at the contact point between the wheel and the ground surface. One must also develop the relationship between the various forces at contact to determine a solution to the dynamic equations of the robot. As in the previous section, we use the Euler-Langrange equations to derive the robot dynamics. In this case of slip we have additional variables and underlying constraints between the variables. The additional variables are the linear longitudinal velocity of the two wheels $(\dot{\rho_r}, \dot{\rho_l})$, the linear lateral velocity $(\dot{\eta})$, and the angular velocities of the wheel $(\dot{\theta_r}, \dot{\theta_l})$. The Langrangian function and is given by

$$\begin{aligned} L = &\frac{1}{2}[m_r(\dot{x_c}^2 + \dot{y_c}^2)] + \frac{1}{2}[I_{rz}\dot{\phi}^2] + \frac{1}{2}[m_w(\dot{\rho_r}^2 + \dot{\eta}^2)] + \frac{1}{2}[m_w(\dot{\rho_l}^2 + \dot{\eta}^2)] \\ &+ \frac{1}{2}[I_{wy}\dot{\theta_r}^2 + I_{wz}\dot{\phi}^2] + \frac{1}{2}[I_{wy}\dot{\theta_l}^2 + I_{wz}\dot{\phi}^2] \end{aligned} \tag{II.22}$$

Since we have additional variables to be considered under slip conditions, the generalized coordinate vector is $q = [x_c, y_c, \phi, \eta, \rho_r, \rho_l, \theta_r, \theta_l]^T$. Figures II.5 and II.6 show the front and lateral views, respectively, of the robot and the various forces involved. We assume the robot is constructed such that its mass is uniformly distributed along the longitudinal axis.

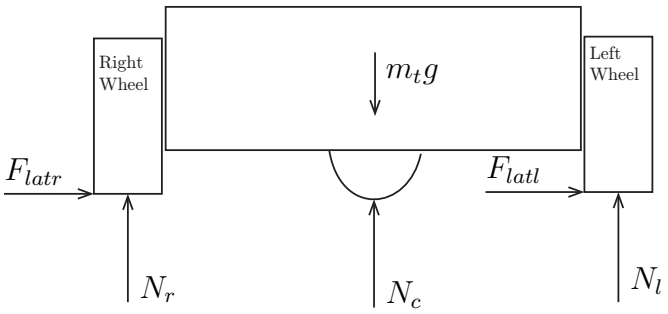

Figure II.5: Front view of the robot showing various forces

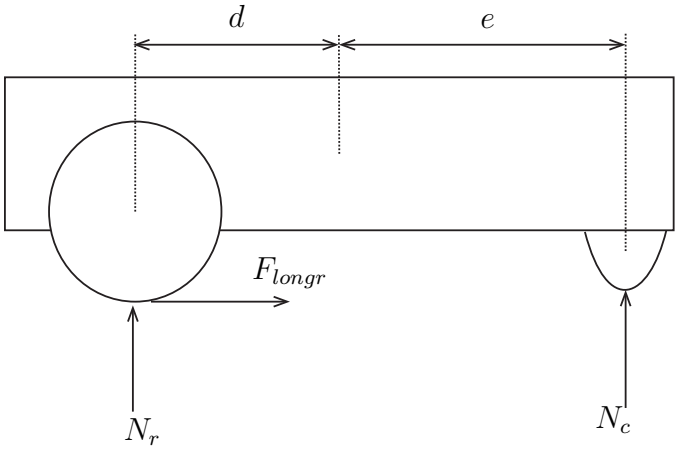

Figure II.6: Lateral view of the robot showing various forces

Therefore, the center mass lies on the longitudinal axis, and we assume it is at a distance "d" from the wheel axis and "e" from the center of the caster wheel.

Note that we assume that the point at which the caster wheel makes contact with the ground surface when projected onto the robot platfom plane falls on the longitudinal axis. Substituting the slip variables $(\dot{\rho}_r, \dot{\rho}_l, \dot{\eta})$ into the Lagrangian and evaluating the Euler-Lagrangian

equations for the variables $(x_c, y_c, \phi, \theta_r, \theta_l)$ we obtain

$$\begin{aligned}
m_t\ddot{x_c} + 2m_w d(\ddot{\phi}\sin\phi + \dot{\phi}^2\cos\phi) &= (F_{longr} + F_{longl})\cos\phi - (F_{latr} + F_{latl})\sin\phi \\
m_t\ddot{y_c} - 2m_w d(\ddot{\phi}\cos\phi + \dot{\phi}^2\sin\phi) &= (F_{longr} + F_{longl})\sin\phi + (F_{latr} + F_{latl})\cos\phi \\
I_t\ddot{\phi} + 2m_w d(\ddot{x_c}\sin\phi + \dot{y_c}\cos\phi) &= (F_{longr} - F_{longl})b - (F_{latr} + F_{latl})d \\
I_{wy}\ddot{\theta_r} &= \tau_r - rF_{longr} \\
I_{wy}\ddot{\theta_l} &= \tau_l - rF_{longl}
\end{aligned} \tag{II.23}$$

The lateral and longitudinal slip dynamics are obtained by differentiating Equations (II.18) with respect to time, the equations are given by

$$\begin{aligned}
\ddot{\rho_r} &= \ddot{x_c}\cos\phi + \ddot{y_c}\sin\phi - \dot{\phi}(\dot{x_c}\sin\phi - \dot{y_c}\cos\phi) + b\ddot{\phi} \\
\ddot{\rho_l} &= \ddot{x_c}\cos\phi + \ddot{y_c}\sin\phi - \dot{\phi}(\dot{x_c}\sin\phi - \dot{y_c}\cos\phi) - b\ddot{\phi} \\
\ddot{\eta} &= -\ddot{x_c}\sin\phi + \ddot{y_c}\sin\phi - \dot{\phi}(\dot{x_c}\cos\phi + \dot{y_c}\sin\phi) - d\ddot{\phi}
\end{aligned} \tag{II.24}$$

Equations (II.23) and (II.24) may be compactly written in matrix form as:

$$M(q)\ddot{q} + C(q, \dot{q}) = B(q)T + F(q) \tag{II.25}$$

where

$$M(q) = \begin{bmatrix} m_t & 0 & 2dm_w \sin\phi & 0 & 0 & 0 & 0 & 0 \\ 0 & m_t & -2dm_w \cos\phi & 0 & 0 & 0 & 0 & 0 \\ 2dm_w \sin\phi & -2dm_w \sin\phi & I_t & 0 & 0 & 0 & 0 & 0 \\ -\sin\phi & \cos\phi & -d & -1 & 0 & 0 & 0 & 0 \\ \cos\phi & \sin\phi & b & 0 & -1 & 0 & 0 & 0 \\ \cos\phi & \sin\phi & -b & 0 & 0 & -1 & 0 & 0 \\ 0 & 0 & 0 & 0 & 0 & 0 & I_{wy} & 0 \\ 0 & 0 & 0 & 0 & 0 & 0 & 0 & I_{wy} \end{bmatrix}$$

$$C(q,\dot{q}) = \begin{bmatrix} 2dm_w\dot{\phi}^2 \cos\phi \\ 2dm_w\dot{\phi}^2 \sin\phi \\ 0 \\ -\dot{\phi}(\dot{x_c}\cos\phi + \dot{y_c}\sin\phi) \\ -\dot{\phi}(\dot{x_c}\sin\phi - \dot{y_c}\cos\phi) \\ -\dot{\phi}(\dot{x_c}\sin\phi - \dot{y_c}\cos\phi) \\ 0 \\ 0 \end{bmatrix} \quad F(q) = \begin{bmatrix} (F_{longr} + F_{longl})\cos\phi - (F_{latr} + F_{latl})\sin\phi \\ (F_{longr} + F_{longl})\sin\phi + (F_{latr} + F_{latl})\cos\phi \\ (F_{longr} - F_{longl})b - (F_{latr} + F_{latl})d \\ 0 \\ 0 \\ 0 \\ -rF_{longr} \\ -rF_{longl} \end{bmatrix}$$

$$B(q) = [O_{6\times 2}, I_{2\times 2}]^T$$

$$T = [\tau_r, \tau_l]^T \tag{II.26}$$

where $O_{6\times 2}$ denotes the 6×2 null matrix and $I_{2\times 2}$ is the 2×2 identity matrix. In addition to the above equations, one can find relationships between various forces, as shown in Figures II.5 and II.6, by using the force and moment balance at the center of mass. These

relationships are given by

$$N_r + N_l + N_c = m_t g \tag{II.27}$$

$$(F_{latr} + F_{latl})h + N_l b = N_r b \tag{II.28}$$

$$N_c(d + e) = m_t g d \tag{II.29}$$

In the following section, we will consider a simple coulomb friction model to relate normal forces with lateral and longitudinal forces at the wheels.

II.4 Traction Forces on Wheels

One must consider the interaction of the wheels with the ground to develop a model for this interaction, which will lead to obtain the solution to the motion equations of the robot. A considerable amount of research in literature has been dedicated to automobile wheels with air filled tires [9], but these models assume either a rigid wheel on a soft ground or a soft wheel on a rigid ground. Further, the models are complex and require several properties of the tires and the ground in order to estimate the interaction between the tire and the ground. These properties are determined through extensive empirical experiments. However, most of the applications in robotics involve rigid wheels on a rigid ground. Therefore, the approach of using a friction model is simple and reasonable for this type of contact between rigid surfaces. In the following, we will describe the traction force model.

Consider a wheel that is rotating without slip as shown in Figure II.7. The equations of motion of the wheel are given by

$$m_w a_w = F_{long} \tag{II.30}$$

$$I_{wy}\ddot{\theta} = \tau - F_{long} r \tag{II.31}$$

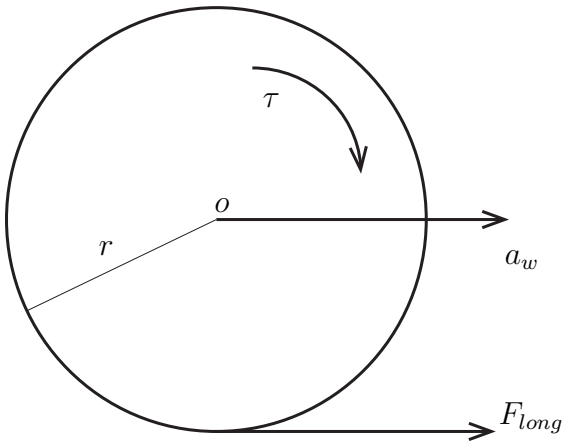

Figure II.7: Wheel rotating without slip

where a_w is the linear acceleration of the wheel.

Under pure rolling conditions the angular acceleration is related to linear acceleration as,

$$a_w = r\ddot{\theta} \tag{II.32}$$

If we consider these equations and express the longitudinal force in terms of applied torque, we obtain

$$F_{long} = \frac{\tau m_w r}{m_w r^2 + I_{wy}} \tag{II.33}$$

Such a simple relation between longitudinal force and applied torque cannot be established when there is slip. In the presence of slip, we consider the Coulomb friction model to establish the relationship between the normal force and the force exerted by the applied torque, due to irregularities of the bodies in contact as shown in Figure II.8 [21].

A static friction coefficient is utilized to determine the value of the maximum force that has to be applied to the wheel before the wheel starts to slip. The necessary force to have a relative movement of the bodies is the largest, because the asperities between the bodies in

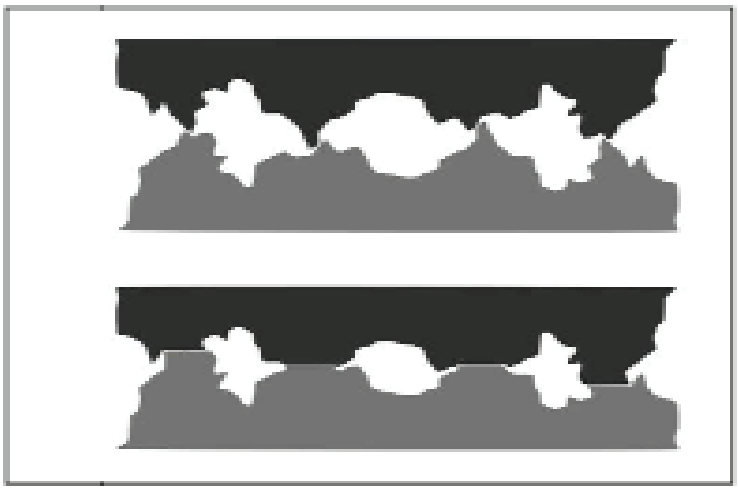

Figure II.8: Asperities of two surfaces before (top) and after (bottom) load is applied

contact act as anchors, and it is necessary to break those anchors in order to slip the bodies relative to each other. Considering μ_s to be the coefficient of static friction and N as the normal force on the wheel, we have

$$F_{long} = \mu_s N \tag{II.34}$$

If the resultant force due to the applied torque is less than the static frictional force, it is completely transmitted to the ground resulting in pure rotation of the wheel. If the resultant force exceeds the static frictional force, a portion of this force that is above the static frictional force causes the wheel to slip (i.e., to rotate without any linear displacement), the remaining force is utilized for the forward motion of the wheel. Hence, slip occurs if the value of F_{long} given by Equation (II.33) is greater than that of Equation (II.34). The force that results in the linear motion is determined by the kinetic friction coefficient and is given by

$$F_{long} = \mu_k N \tag{II.35}$$

Lateral slip of the wheel may occur in conjunction with longitudinal slip. In order to determine the actual relation between the amount of slip and the force applied, we decompose the total force due to the applied torque into lateral and longitudinal force components as shown in Figure II.9. Decomposing the total force ($\mu_k N$) into longitudinal and lateral forces,

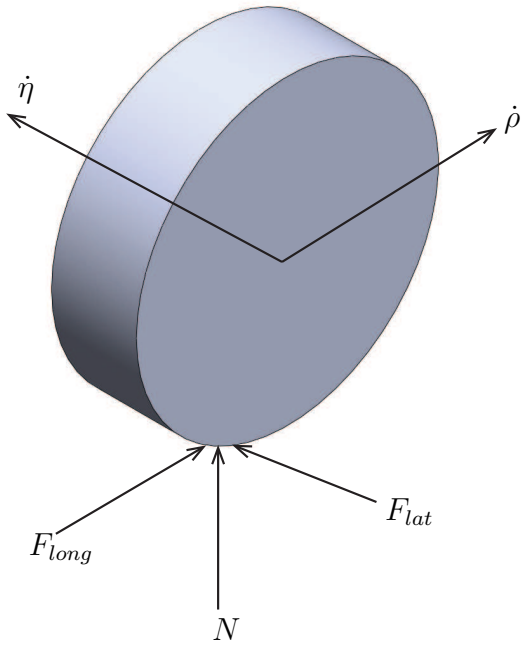

Figure II.9: Longitudinal and lateral slip due to friction forces

we obtain

$$F_{longr} = \mu_k N_r \left(\frac{\dot{\rho}_r}{\sqrt{\dot{\rho}_r{}^2 + \dot{\eta}^2}}\right) \tag{II.36}$$

and

$$F_{latr} = \mu_k N_r \left(\frac{\dot{\eta}}{\sqrt{\dot{\rho}_r{}^2 + \dot{\eta}^2}}\right) \tag{II.37}$$

$$F_{longl} = \mu_k N_l \left(\frac{\dot{\rho}_l}{\sqrt{\dot{\rho}_l{}^2 + \dot{\eta}^2}}\right) \tag{II.38}$$

and

$$F_{latl} = \mu_k N_l \left(\frac{\dot{\eta}}{\sqrt{\dot{\rho_l}^2 + \dot{\eta}^2}}\right) \tag{II.39}$$

where the subscript r and l are used to refer to the right and left wheel, respectively.

II.5 Robot Control

In this section a trajectory tracking controller for the differential drive robot under wheel slip is investigated. A two loop structure as shown in Figure II.10 is used when a path following controller proposed in [1] is used for path correction which forms the outer loop and the inner loop controller converts the path correction into motor torques for the differential wheels. The kinematic controller uses the robot's desired position and the actual position to compute the necessary velocity corrections. These velocity corrections are used to computed the required wheel torques for the differential drive. If the torques create a linear force greater than the force given by Equation (II.34), then a slip avoidance controller is used to prevent the wheels from slipping by limiting the input torque.

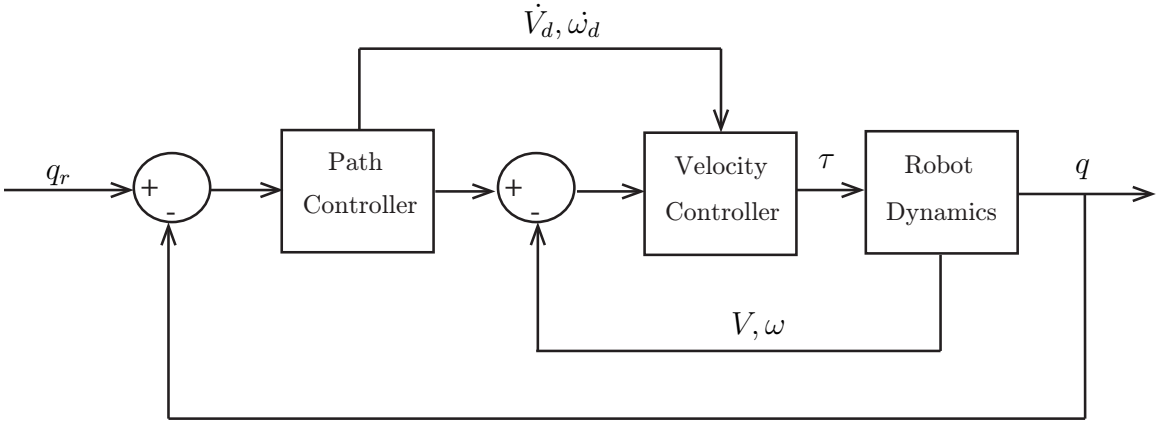

Figure II.10: Control block diagram

II.5.1 Robot Control under Pure Rolling

Consider a robot that is traveling on a reference trajectory as shown in Figure II.11. Let q_r be the reference position of the robot and q be the actual position where $q_r = [x_r, y_r, \phi_r]^T, q = [x, y, \phi]^T$, respectively. Then the robot position and orientation error are given by

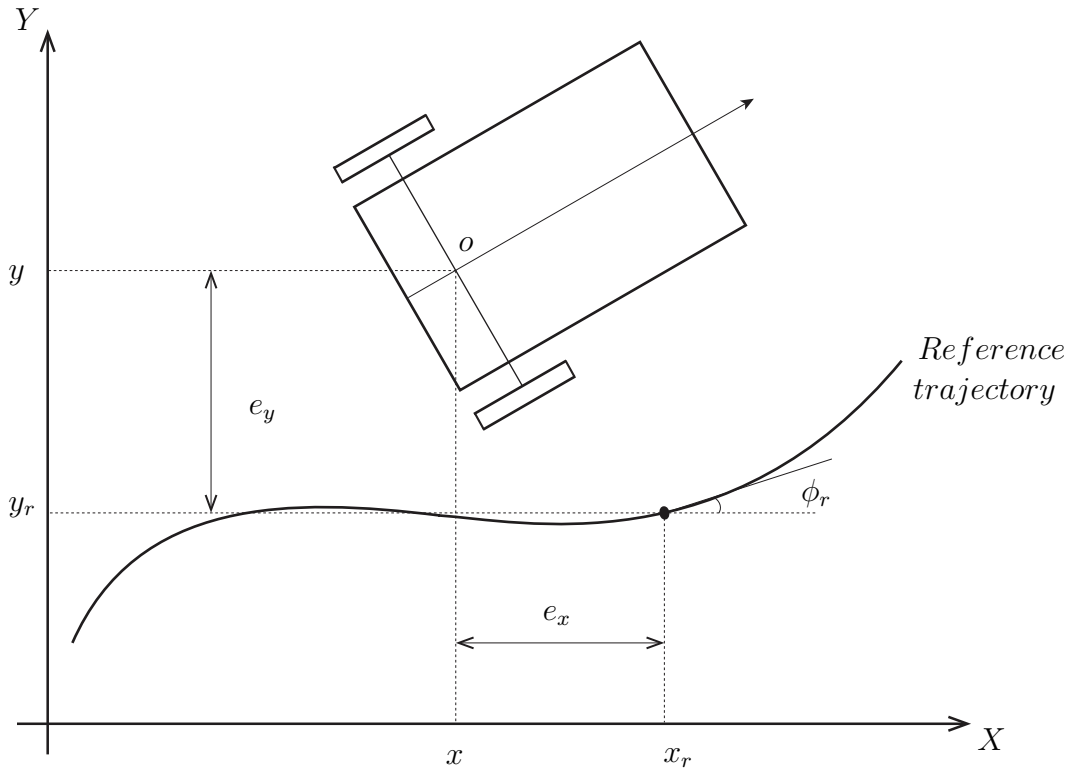

Figure II.11: Trajectory tracking robot model

$$\begin{bmatrix} e_x \\ e_y \\ e_\phi \end{bmatrix} = \begin{bmatrix} \cos\phi_r & \sin\phi_r & 0 \\ -\sin\phi_r & \cos\phi_r & 0 \\ 0 & 0 & 1 \end{bmatrix} \begin{bmatrix} x - x_r \\ y - y_r \\ \phi - \phi_r \end{bmatrix} \tag{II.40}$$

Differentiating the position errors we obtain the error dynamics

$$\begin{bmatrix} \dot{e}_x \\ \dot{e}_y \\ \dot{e}_\phi \end{bmatrix} = \begin{bmatrix} \omega_d e_y - v_d + v_r \cos e_\phi \\ -\omega_d e_x + v_r \sin e_\phi \\ \omega_r - \omega_d \end{bmatrix} \tag{II.41}$$

The control objective is to select v_d and ω_d such that the error equilibrium solutions, $e_x = 0, e_y = 0, e_\phi = 0$, are stable. Lyapunov's second method to select v_d and ω_d. Consider the following Lyapunov function candidate:

$$V = \frac{1}{2}(e_x^2 + e_y^2) + \frac{1}{k_y}(1 - \cos e_\phi) \tag{II.42}$$

It is easy to see that the above Lyapunov function candidate is strictly positive for all non-zero errors. Taking the time derivative of V along the solution trajectories of Equation (II.41), we obtain

$$\dot{V} = (v_r \cos(e_\phi) - v_d)e_x + \frac{1}{k_y}(\sin(e_\phi))(k_y v_r e_y + \omega_r - \omega_d) \tag{II.43}$$

If the desired linear and angular velocities are

$$\begin{aligned} v_d =& v_r \cos e_\phi + k_x e_x \\ \omega_d =& \omega_r + v_r k_y e_y + k_\phi \sin e_\phi \end{aligned} \tag{II.44}$$

where k_x, k_y and k_ϕ are positive gains, then $\dot{V}$ is negative semi-definite,

$$\dot{V} = -k_x e_x - \frac{k_\phi}{k_y} \sin^2(e_\phi) \tag{II.45}$$

This implies convergence of e_x and e_ϕ to zero. Using LaSalle's principle, one can show convergence of e_y to zero; see [1] for details.

The desired velocities from Equation (II.44) are the input to the velocity controller that will generate the necessary wheel torques. Define velocity errors $e_v = v_d - v$ and $e_\omega = \omega_d - \omega$. If v and ω are the actual linear and angular velocities of the robot, the velocity error dynamics are given by

$$\begin{aligned} \dot{e}_v &= \dot{v}_d - \frac{\tau_L}{m_t}, \\ \dot{e}_\omega &= \dot{\omega}_d - \frac{\tau_A}{I_t} \end{aligned} \tag{II.46}$$

If we select the torques τ_L and τ_A as

$$\begin{aligned} \tau_L &= m_t \dot{v}_d + k_l(v_d - v), \\ \tau_A &= I_t \dot{\omega}_d + k_a(\omega_d - \omega) \end{aligned} \tag{II.47}$$

then the velocity error equations are given by

$$\begin{aligned} m_t \dot{e}_v + k_l e_v &= 0, \\ I_t \dot{e}_\omega + k_a e_\omega &= 0 \end{aligned} \tag{II.48}$$

The choice of gains k_l and k_a to be positive will imply that $e_v = 0$ and $e_\omega = 0$ are exponentially stable. Using Equation (II.12), the wheel torques are given by

$$\begin{aligned} \tau_l &= \left(\tau_L + \frac{1}{2b}\tau_A\right) r/2, \\ \tau_r &= \left(\tau_L - \frac{1}{2b}\tau_A\right) r/2 \end{aligned} \tag{II.49}$$

As discussed before these torques are computed considering pure rolling conditions. In the next section we use these torques to verify the onset of slip and limit the torques to avoid slip.

II.5.2 Robot Control to Avoid Slip

When the total applied torque is not transmitted to the ground, then there is slip. Based on the traction force model, if we limit the applied torque such that the reaction force is less than the maximum allowable friction force, we can avoid slip. The strategy is used to limit the applied torque during motion control. Recall that the relation between the longitudinal force and the torque on a wheel is obtained from Equation (II.33). The longitudinal force acting on a single wheel of the robot is given by

$$F_{long} = \frac{\tau \frac{m_t}{2} r}{\frac{m_t}{2} r^2 + I_{wy}} = \frac{\tau m_t r}{2I_{wy} + m_t r^2} \tag{II.50}$$

Note that the above equations is different from Equation (II.33) as we use the portion of the robot mass that is acting on the wheel. As it was pointed before, this force must be less than the force given by the static coefficient of friction. Then, in order to avoid slip, we limit the f_{long} in Equation (II.50) to $\mu_s N$. Then, the maximum torque that can be applied to the wheel to ensure that there is no slip, is given by

$$\tau_{max} = \frac{\mu_s N(2I_{wy} + m_t r^2)}{m_t r} \tag{II.51}$$

The normal force N in the above equation is either N_r or N_l depending on the application of this to either the right or the left wheel. This value of torque is compared to the one generated by the controller by Equation (II.49). If the torques τ_l or τ_r are less than their

corresponding maximum values, then the torques are applied directly. If the applied torque is greater, the values of the applied torques are limited to the maximum allowable.

The block diagram of this applied control system is shown in Figure II.12. The error between

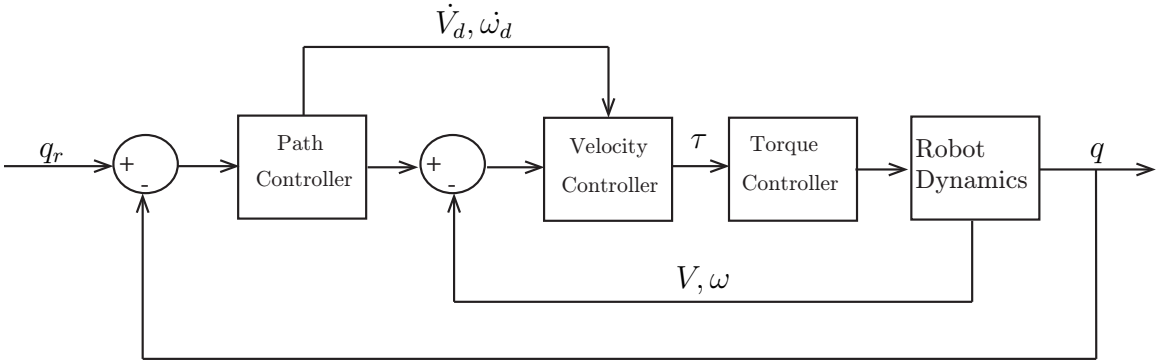

Figure II.12: Control block diagram

the reference position and the actual position given by the encoders generates the desired velocities in the kinematic controller using the nonlinear path controller developed before, Equation (II.41). These desired velocities are compared to the actual velocities of the robot in the velocity controller. Using Equation (II.49) the desired wheel applied torques are produced. However, these torques are compared to the maximum torque that can be applied prior to the occurrence of slip, Equation (II.51). If the applied torque is greater than the maximum torque, then they are limited to this value. This is compared and limited in the torque controller block, before the torques are transmitted to the actuators.

The necessary equations that will be used in the simulations have been developed. We begin with a model of the robot, followed by the kinematics and dynamics under pure rolling conditions slip conditions. Then, a traction force model was developed in order to overcome the lack of information and the difficulty of experimentation to determine the exact properties of the interaction between the wheels and the ground. Once, this dynamics behavior is established, the controller to avoid slip is develop. Model simulations are described in the

Table II.2: Simulation Variables

Symbol	Value	Unit
μ_s	0.241	
μ_k	0.239	
$2b$	0.21	m
e	0.095	m
d	0.055	m
g	9.81	m/s
h	0.0216	m
m_r	1.5	kg
I_{rz}	0.009753	kg m^2
I_{wz}	0.000584	kg m^2
I_{wy}	0.001168	kg m^2
r	0.0365	m
m_w	0.064	kg

next section.

II.6 Model Simulations

Numerical simulations are conducted using MATLAB/Simulink software to learn the behavior of the proposed robot dynamics with slip for a range of input torques. The values of the parameters used in these simulations are shown in Table II.2. Using the numerical values given in Table II.2, the value of the maximum allowable torque that can be applied to the system to avoid slip is 0.095 m-N. The first set of simulations is conducted to compare the robot model under slip with the robot model under pure rolling conditions [3]. The second set of simulations is carried out to observe the response of the proposed model with a practical torque profile where a constant torque is applied for a small duration of time. The third set is to observe the response of the system when torque limiting control is implemented.

II.6.1 Comparison of the Slip and Pure Rolling Models

To evaluate the response of the dynamic models with and without slip, three different values of constant torques are applied to the two models. The magnitude of the first set of applied torques (0.09 m-N) is less than the magnitude of the maximum allowable torque to produce slip. The position response of both models is shown in Figure II.13. From the figure it is evident that the response of both models is the same. This shows that the slip model has a proper response under pure rolling conditions, that is, the response of the model that includes slip is identical to the model with pure rolling assumption when the maximum allowable torque is below the threshold value that produces slip. The magnitude of the second set of torques (0.1 m-N) is greater than the maximum allowable torque. From the response shown in Figure II.14, it is evident that the proposed model is capable of capturing slip. As expected the distance that the robot travels under slip conditions is less than the distance traveled under pure rolling condition. Simulations with torque value of 0.3 m-N are shown in Figure II.15; note that this torque level is three times bigger than the minimum value of torque to produce slip. It is evident that if the robot slips significantly, the actual distance traveled by the robot is significantly less than the distance traveled under pure rolling conditions. Notice that once the robot slips the distance that the robot travels is similar even if the torque magnitudes are different. This is because the portion of the energy needed to move the robot is same for any torque magnitude above the maximum.

II.6.2 Simulations with a Velocity Profile

In the previous section a step input was given to the system, such an input cannot be continuously applied in practice. A more realistic input based on a velocity profile for a straight line trajectory is used. The robot is accelerated for 0.5 seconds, after which the

velocity is maintained at a constant value. This velocity profile is used as a reference to the closed-loop system and the proposed model is simulated to observe its response. Three sets of velocity profiles are used to mimic the conditions where the torque required is below the maximum allowable torque limit (0.09 m-N), above this limit (0.1 m-N), and at the maximum rated torque of the motors (0.13 m-N).

For all the cases the wheel angular velocity and the linear velocity of the robot are shown in Figures II.16 through II.21. These responses will be compared with the experimental results shown in the next chapter. Notice that the distance traveled before slip occurs at 44 rad/s^2 is greater than the distance traveled at 48 rad/s^2; from Figures II.17 and II.19 one can observe that the distance traveled is more in the case of 44 rad/s^2. However, when the torque is increased further (72 rad/s^2), there is no appreciable change in the distance traveled by the robot (compare Figures II.17 and II.21)

II.6.3 Closed-Loop Simulations with Torque Limiting Control

The control strategy developed in Section II.5 is used to avoid slip by keeping the applied torque smaller than the maximum torque to produce slip for any acceleration profile. The closed loop system with the torque controller is simulated for a reference acceleration of 72 rad/s^2 for 0.5 s. This acceleration was chosen based on the fact that it is greater than the maximum acceleration required for the wheel to slip. For the sake of comparison, simulations are carried out with and without the torque limiting controller. The simulations without the torque controller are shown in Figure II.22 for the chosen acceleration. The simulation with the proposed torque limiting control is shown in Figure II.24 and the error in the trajectory with the torque control is shown in Figure II.25. The position trajectory error is shown in Figure II.23 where we can see the maximum value of error is 0.3 m. Notice that the error

with the torque limiting control is 0.16 m, which is almost half of the error without the torque limiting control.

In this chapter models for the dynamics under pure rolling conditions and slip conditions have been developed. A force traction model was developed by considering the linear and lateral velocities of the wheels, static and kinetic friction, the caster wheel. From the model the maximum allowed torque to avoid slip was determined and a torque limiting control strategy to avoid slip was presented. Model simulations and closep-loop system simulations were conducted to evaluate the response under different scenarios.

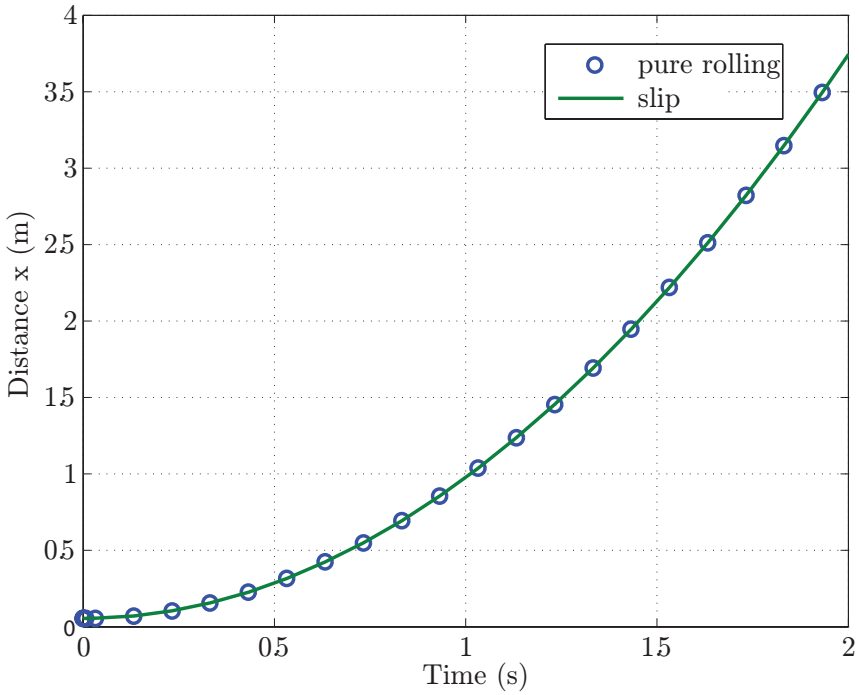

Figure II.13: Straight line trajectory: Torque value = 0.09 m-N

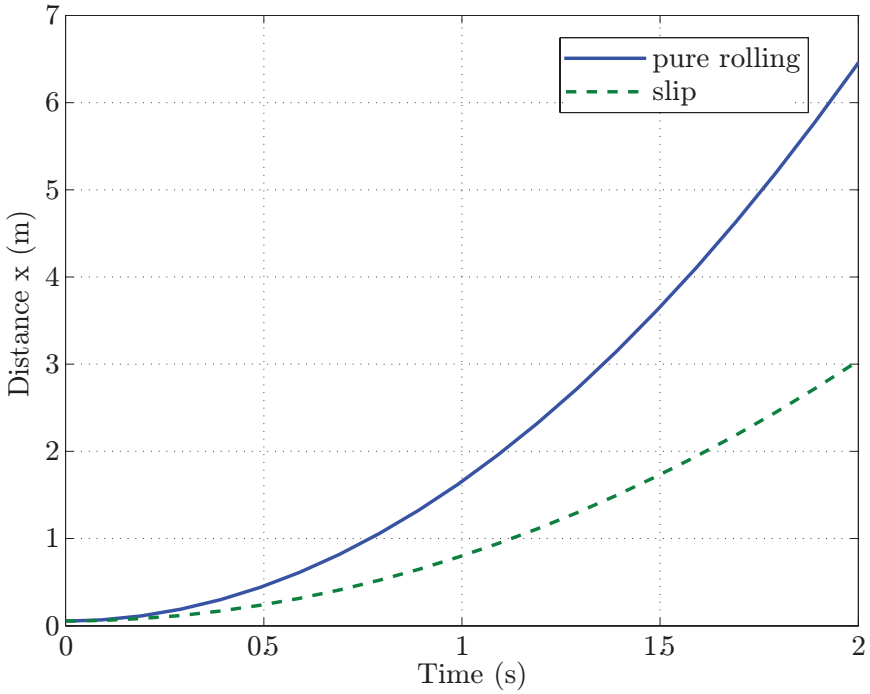

Figure II.14: Straight line trajectory: Torque value = 0.1 m-N

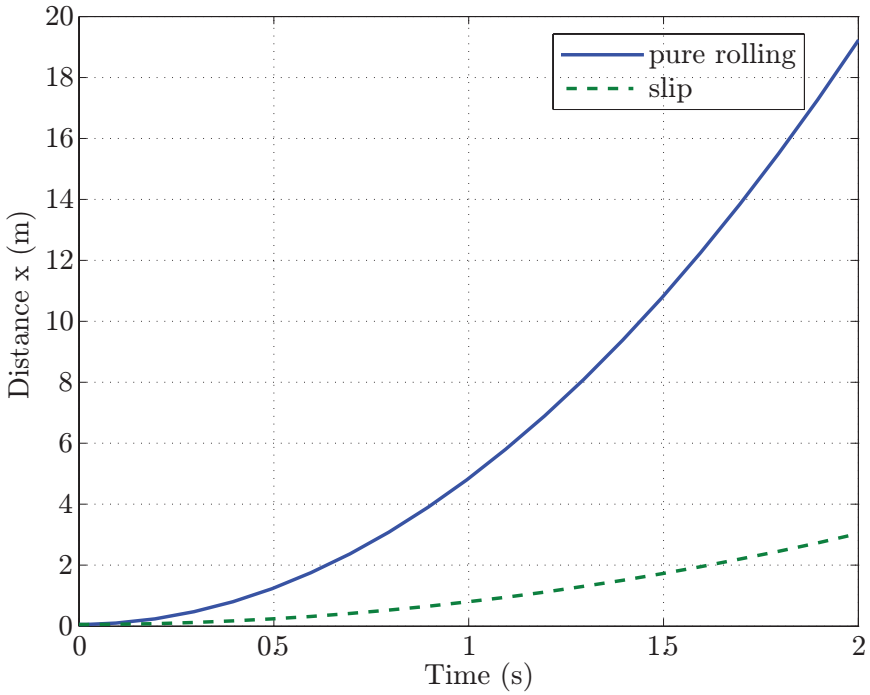

Figure II.15: Straight line trajectory: Torque value = 0.3 m-N

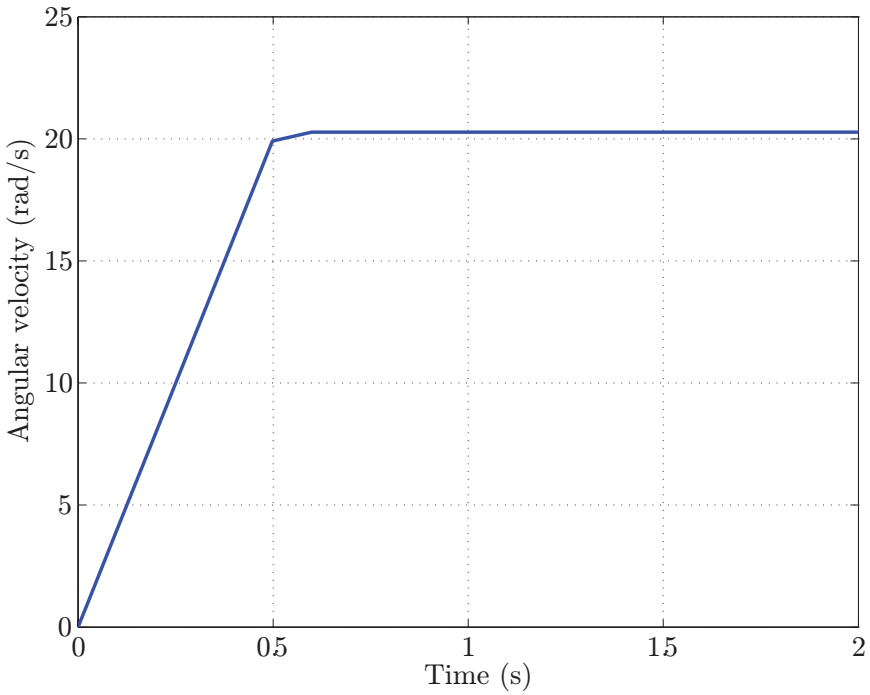

Figure II.16: Wheel angular velocity for torque = 0.09 m-N and acceleration = 44 rad/s^2

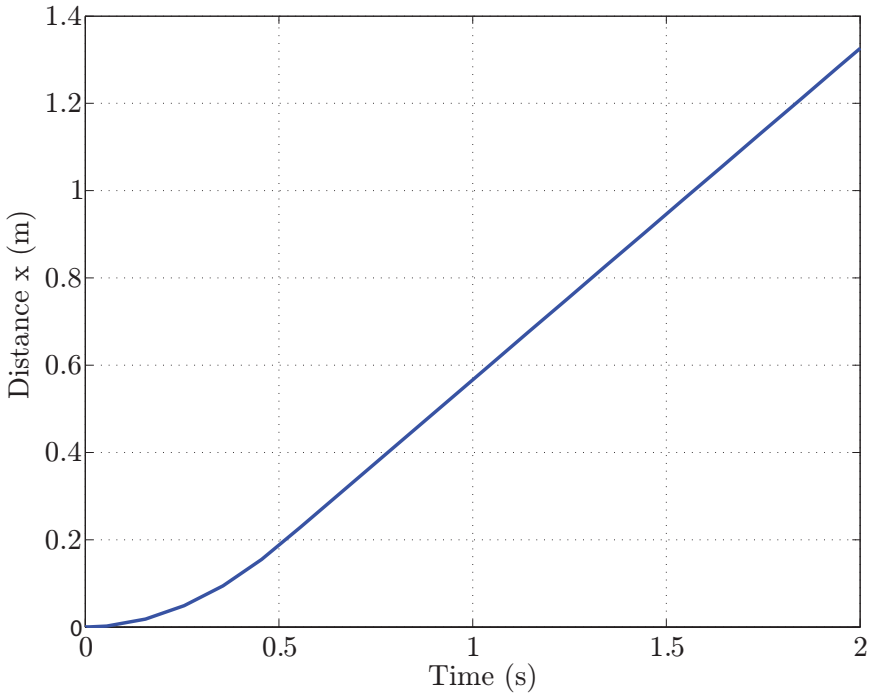

Figure II.17: Position of the robot for torque = 0.09 m-N, acceleration = 44 rad/s^2

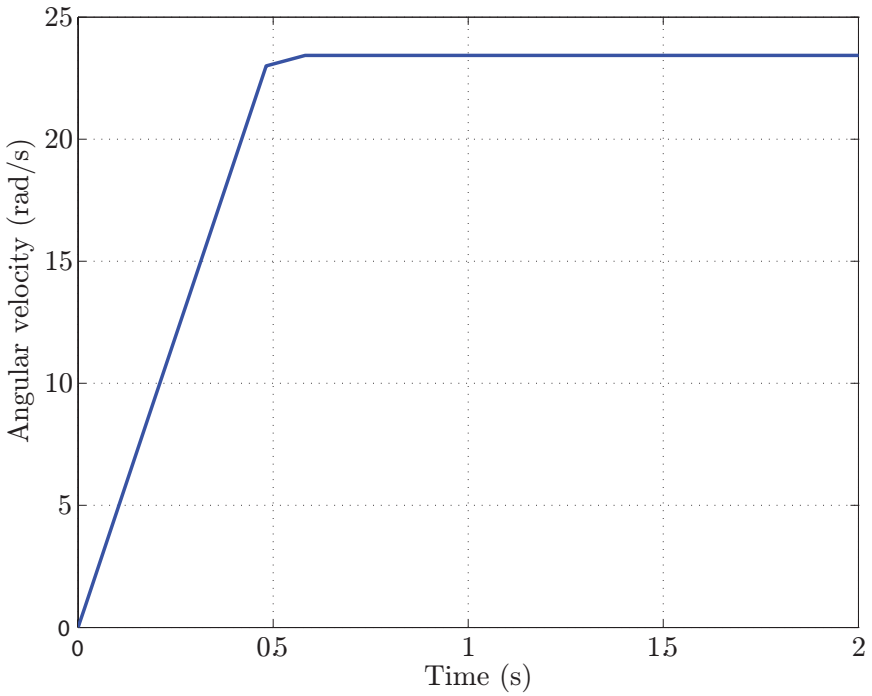

Figure II.18: Wheel angular velocity for torque = 0.1 m-N and acceleration = 48 rad/s^2

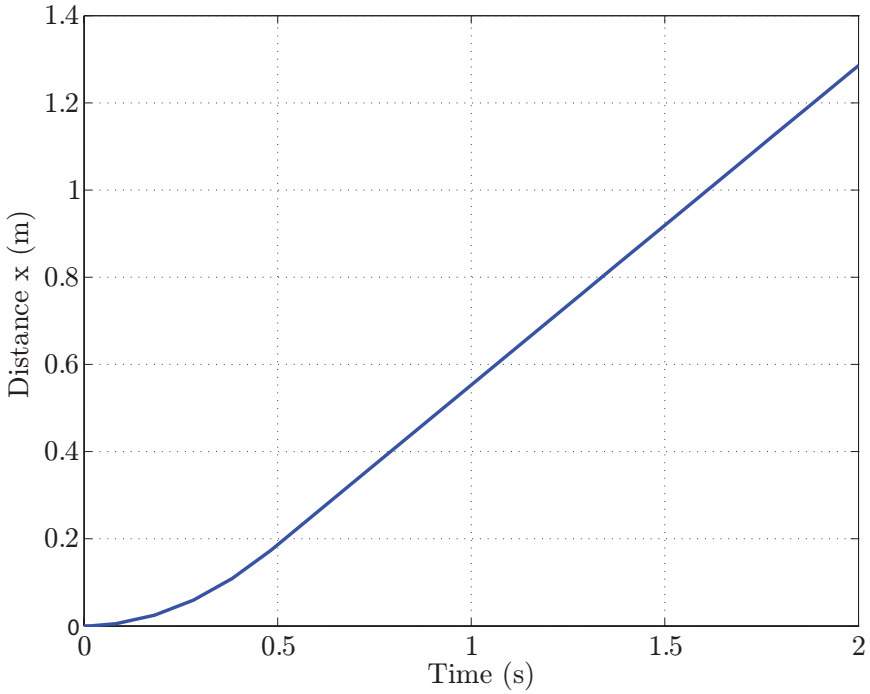

Figure II.19: Position of the robot for torque = 0.1 m-N, acceleration = 48 rad/s^2

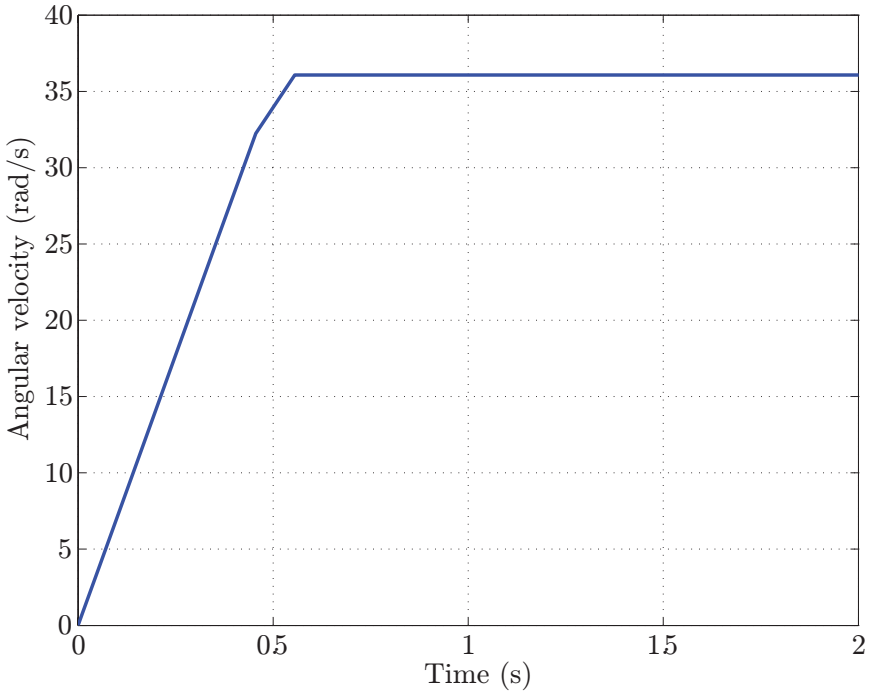

Figure II.20: Wheel angular velocity for torque = 0.13 m-N and acceleration = 72 rad/s^2

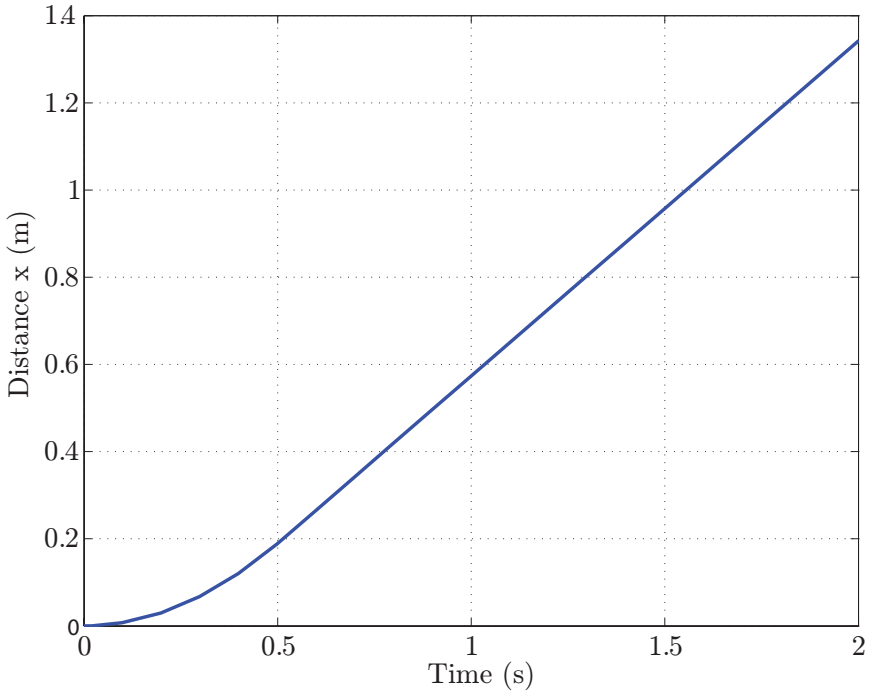

Figure II.21: Position of the robot for torque = 0.13 m-N, acceleration = 72 rad/s^2

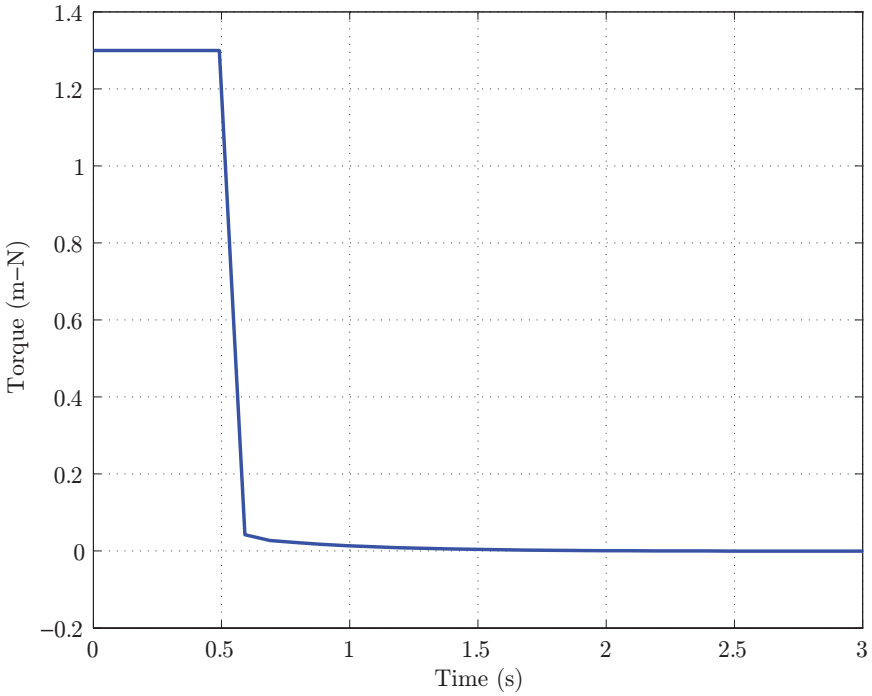

Figure II.22: Torque profile without torque limiting control

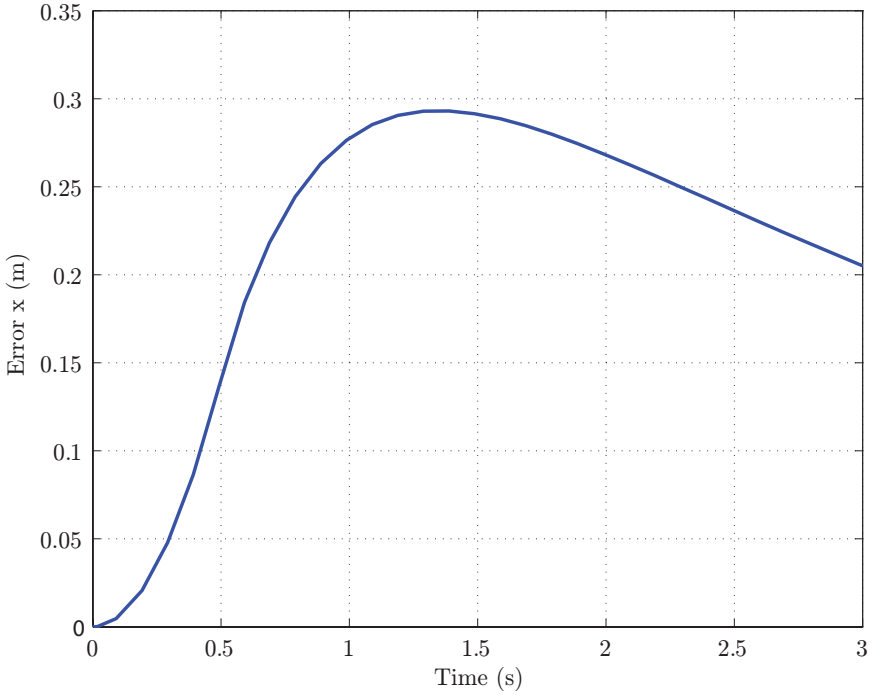

Figure II.23: Position trajectory error without torque limiting control (reference= 72 rad/s^2)

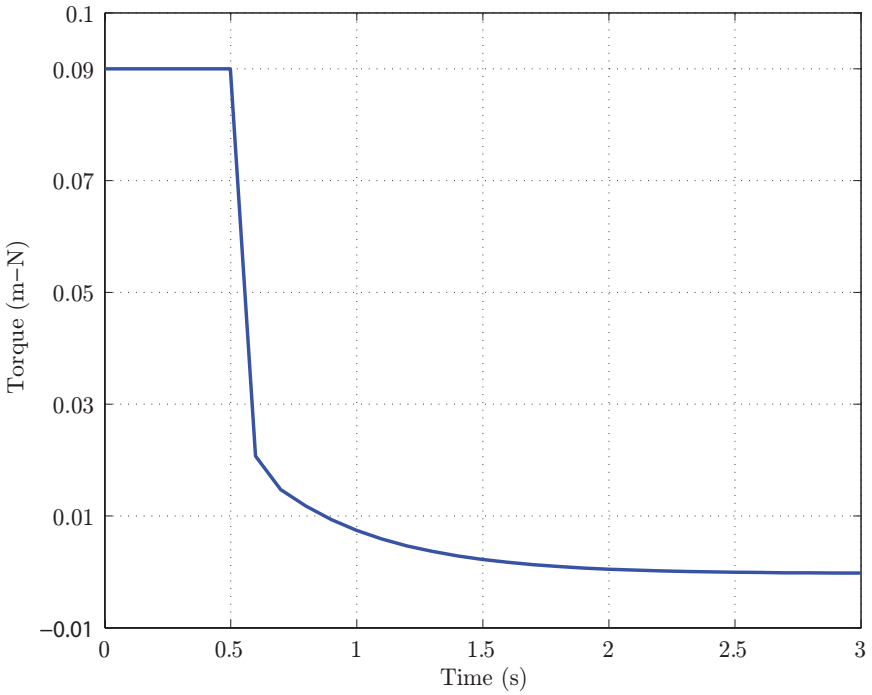

Figure II.24: Torque profile with torque limiting control(reference = 72 rad/s^2)

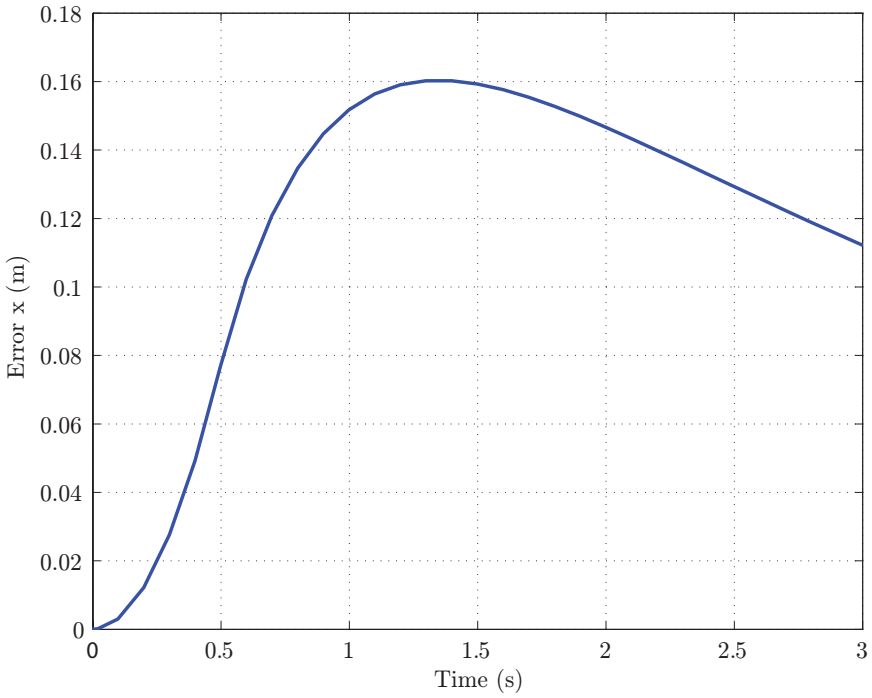

Figure II.25: Position trajectory error with torque limiting control (72 rad/s^2)

CHAPTER III

EXPERIMENTS WITH A DIFFERENTIAL DRIVE ROBOT

Experiments were conducted to verify the characteristics of the dynamic model with slip and the torque limiting control strategy used to avoid slip. Details of the differential drive mobile robot setup used to conduct the experiments are given first followed by the a discussion of the results from the experiments.

III.1 Differential Drive Robot Setup

The differential drive robot has three main components: base or platform with actuators, real-time controller and wireless modules, and encoders to measure wheel angular position. Each component is explained in detail in the following section.

III.1.1 Robot Base and Actuators

The two driven wheels are placed at the back of the base plate to avoid wheel lift off on uneven surfaces. The caster wheel is placed in the front to maintain balance of the robot. In order to keep the center of gravity of the entire robot close to the center of the plate, the battery (the heaviest component) is placed between the wheels on the center line of the base.

The base of the robot is an aluminum plate with length 0.22 m (9 in), width 0.18 m (7 in), and thickness 0.03 m (0.1 in). The two motors that power the wheels are mounted over the base plate, in order to avoid deformation of the plate, and to keep the center of gravity close to the ground. The wheels are directly mounted on the motor shafts. A steel ball caster wheel is used. The battery is mounted between the motors along the longitudinal axis of the platform in such a manner that it is easy to charge it without removing it from the robot.

Identical DC motors are used to power the two wheels. The DC motor has the following specifications: no-load rated speed of 350 RPM (36 rad/s), stall torque of 0.77 N-m, 12 V supply with 2 A maximum current. An encoder with 1856 pulses per revolution is mounted on the motor shaft. The entire robot weighs about 1.63 kg. Figure III.1 shows a picture of the mobile robot.

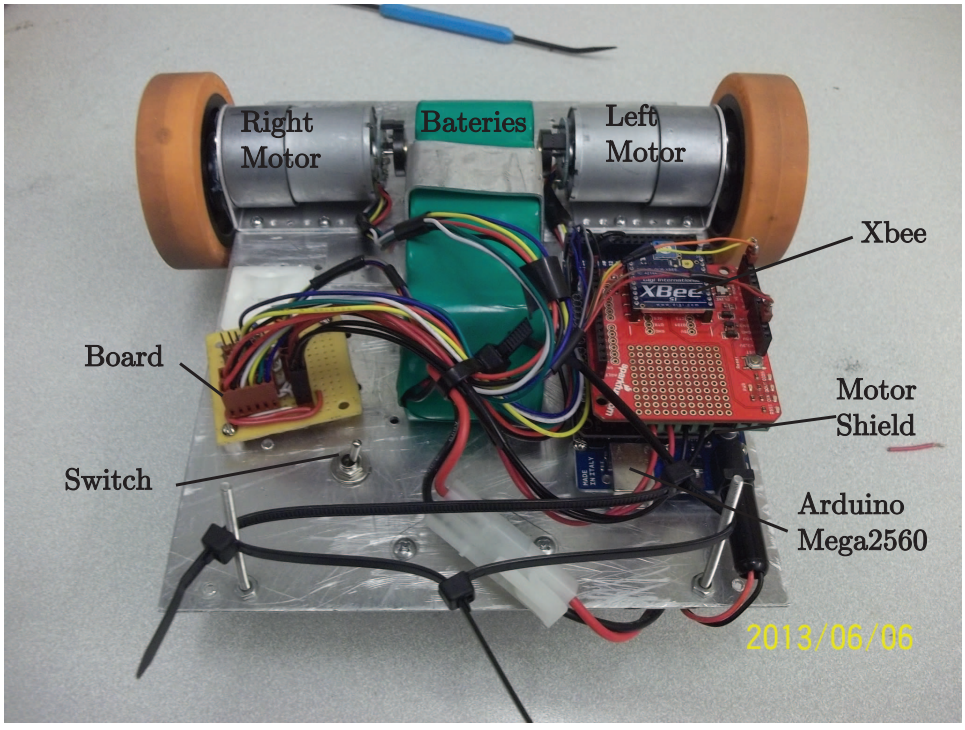

Figure III.1: Robot top view

III.1.2 Real-time Controllers and Wireless Modules

The control algorithm is implemented on the Arduino Mega 2560 real-time board which has the following features: 256 KB of flash memory, 8 KB of SRAM and 4 KB of EEPROM, 16 MHz clock speed, 8-bit PWM output, 6 external interrupt pins and I2C communication interfaces [24]. The board can be connected to a PC via USB and contains two internal voltage regulators of 5 V and 3.3 V. The board can operate from an external supply between 6-20 V and has a USB over-current protection. It can be programmed using Arduino Software Development Kit [25]. Figure III.2 shows an Arduino Mega 2560 board. The Arduino

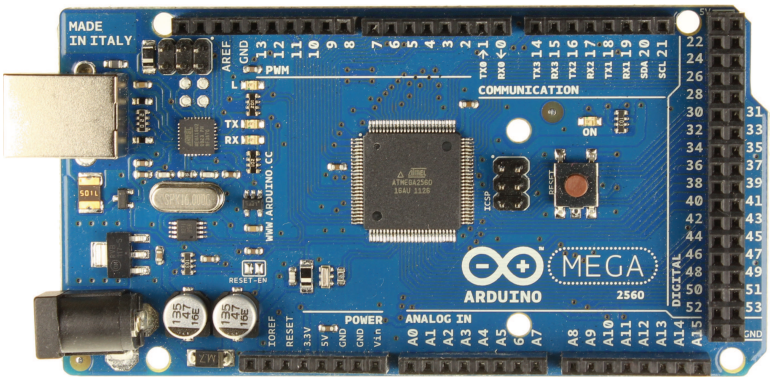

Figure III.2: Arduino Mega 2560

board takes the direction and velocity wave pulse modulation(WPM) signals and with the help of an Arduous Motor shield generates the voltages required to run the motors. An Arduino Motor shield is shown in Figure III.3. A 2.4 GHz Xbee 802.15.4 module from Digi is used for wireless communication, [26]. The Xbee module operates at 3.3 V @ 50 mA. It transmits data at a maximum rate of 250 kbps. It has a range of 300 ft and has a 128-bit encryption. Together these modules can process the control algorithm, compute the reference positions and velocities, control the motors, obtain data from the encoders using external interrupts, and communicate wirelessly with a host PC to transfer data for analysis. A real-time algorithm is programmed on the board to achieve all these tasks. The inner torque

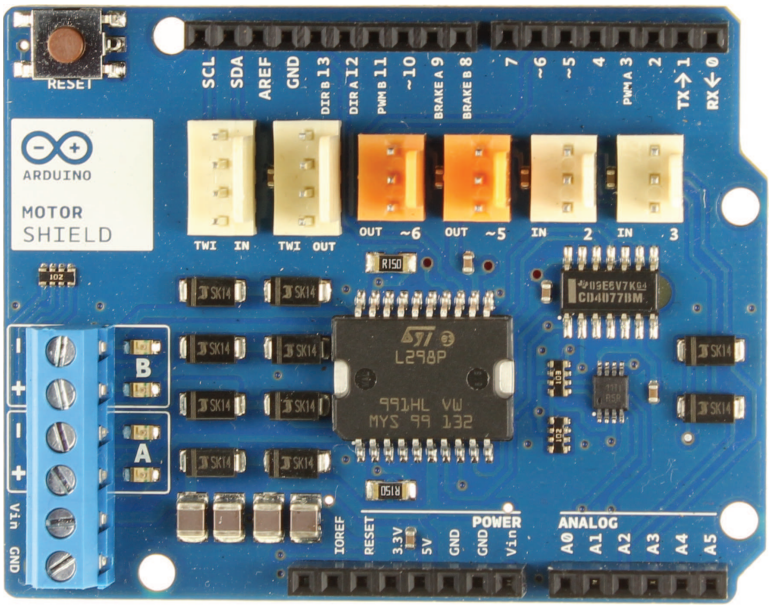

Figure III.3: Motor Shield

loop runs every 25 milliseconds and the outer kinematic loop runs every 50 milliseconds. Measured and computed data, such as encoder signals, robot position and velocity, torque input, etc., are sent via wireless communication to the host PC every 20 milliseconds.

III.1.3 Robot Position Sensing

The encoders on the motor shafts act as the primary position sensors. Each encoder is powered by a 5 V supply and has two data channels A and B. The voltage in the channels is either 5 V or 0 V and it pulsates as the motor shaft rotates. Channels A and B of the encoders are connected to different pins (left: 20, 21; right: 18, 19), which can function as external interrupt pins. The state in the pins changes when the voltage in the channel changes. An interrupt sub-routine is executed every time the pins change their states. This sub-routine counts the number of pulses in both the channels and the direction of the rotation, comparing the sequence in which the pins change their respective states. The encoders provide a measurement of the angular position as the wheel rotates. To compute

the angular velocity of the wheel, we count the number of encoder pulses in time δt. Let N be the number of pulses in time δt. Since the encoder resolution is 1856 pulses per revolution, we obtain the velocity as

$$\dot{\theta} = \frac{2\pi N}{1856\delta t}\text{rad/s} \tag{III.1}$$

The angle for a given time is calculated using the time interval δt and the linear velocities of the wheels using the following relationship

$$\phi(t) = \phi(t - \delta t) + (v_r - v_l)\delta t/2b \tag{III.2}$$

Then, the displacement of the robot in the time interval δt is calculated and added to the previous position, which gives the position of the robot at time t as

$$x(t) = x(t - \delta t) + \frac{b(v_r + v_l)(\sin(\phi(t)) - \sin(\phi(t - \delta t)))}{(v_r - v_l)} \tag{III.3}$$

$$y(t) = y(t - \delta t) + \frac{b(v_r + v_l)(\cos(\phi(t)) - \cos(\phi(t - \delta t)))}{(v_r - v_l)} \tag{III.4}$$

The linear position calculated from the encoders will provide position errors due to the wheel slip. For this reason the position determined by the encoders is only true under pure rolling conditions.

In experiments, due to slip, the robot position computed using the encoder signals is not the actual position. One must device another mechanism to measure the actual robot position when there is wheel slip. A video camera is used to capture the video of each experiment and frames are processed (using image processing in MATLAB) to obtain the actual position of the robot.

III.2 Experimental Results

Three different experiments are carried out with the differential drive robot: (i) estimation of static and kinetic friction coefficients, (ii) experiments at different levels of wheel accelerations to investigate the validity of the traction force model, and (iii) application of the torque limiting control algorithm to verify whether slippage is avoided. For all the mobile robot controlled motion experiments, the actual global position of the robot was obtained using the video.

III.2.1 Estimation of Friction Coefficients

Although more accurate methods are available to compute the friction coefficients, a simple method is employed that requires the use of a simple spring-type weighing scale. The mobile robot and the weighing scale are shown in Figure III.4. A gradually increasing force is applied and the value of the force at which the wheel starts to move is recorded as the static friction force and this is used to calculate the coefficient of static friction. Once the wheels starts moving the force required to keep it moving is recorded to calculate the coefficient of kinetic friction. This procedure was repeated 20 times and the values of the coefficients were calculated for each trial. The value of static coefficient and kinetic coefficient for these trials are shown in Figure III.5 and III.6, respectively. Data from several trials are discarded and the average is computed. The average value of static friction coefficient is 0.241 and that of the kinetic friction coefficient is 0.239.

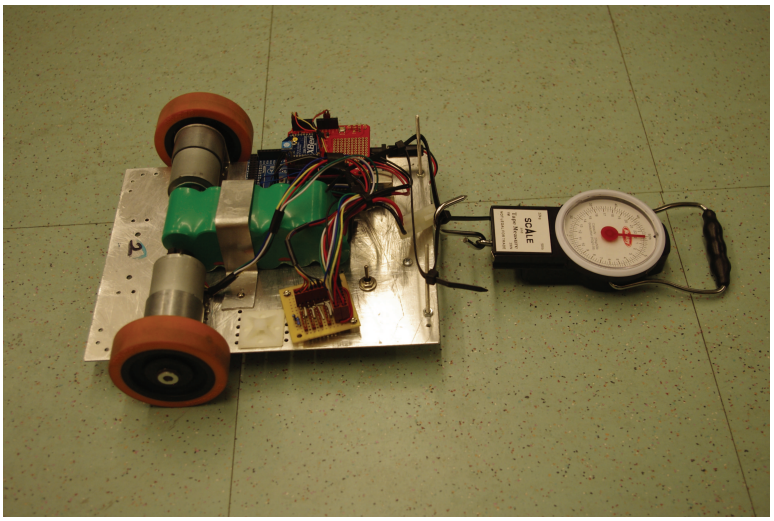

Figure III.4: Setup to determine the coefficient of friction

III.2.2 Traction Force Model Validation

Several experiments were conducted with different accelerations to determine when the slippage occurs. The same acceleration profiles used in model simulations in the previous chapter were also used in the experiments. The following procedure was employed to run each of the motion experiments: (1) The robot was positioned at the same location on the ground at the start of each experiment. (2) The camera placed on the ceiling was activated remotely at the start of each motion experiments. (3) Data recorded from the encoders is transmitted to the host computer. (4) The robot and the video record are deactivated.

The following three reference acceleration levels were employed: 44, 48, and 72 rad/s^2. As in the case of model simulations, each level of acceleration is applied for 0.5 seconds and then a constant velocity is maintained by resetting the reference acceleration to zero. For the reference acceleration case of 44 rad/s^2, Figure III.7 shows the evolution of the wheel angular velocity and Figure III.8 shows the robot position obtained from encoder and video measurements. note that in this case the robot position measured by the camera and the encoders are similar. Therefore, at the acceleration level of 44 rad/s^2, the wheels are not

slipping. The corresponding results for the other two cases (48 and 72 rad/s^2) are shown if Figures III.9 through III.12; note that in these two cases the mobile robot is clearly slipping as the robot position based on encoder measurement lags the one obtained from camera measurements. For slower speeds, the wheel angular velocity shows oscillations; this may be due to the response of the motor which was not taken into consideration in the development of the controller.

III.2.3 Torque Limiting Control Strategy

Experiments were conducted by employing the torque limiting control strategy given in Section II.5.2. Figure III.13 shows the wheel angular velocity. Figure III.14 shows the robot position as obtained from encoders and video measurements, which are similar to each other. Due to limiting of the torque, wheel acceleration is limited to avoid slip.

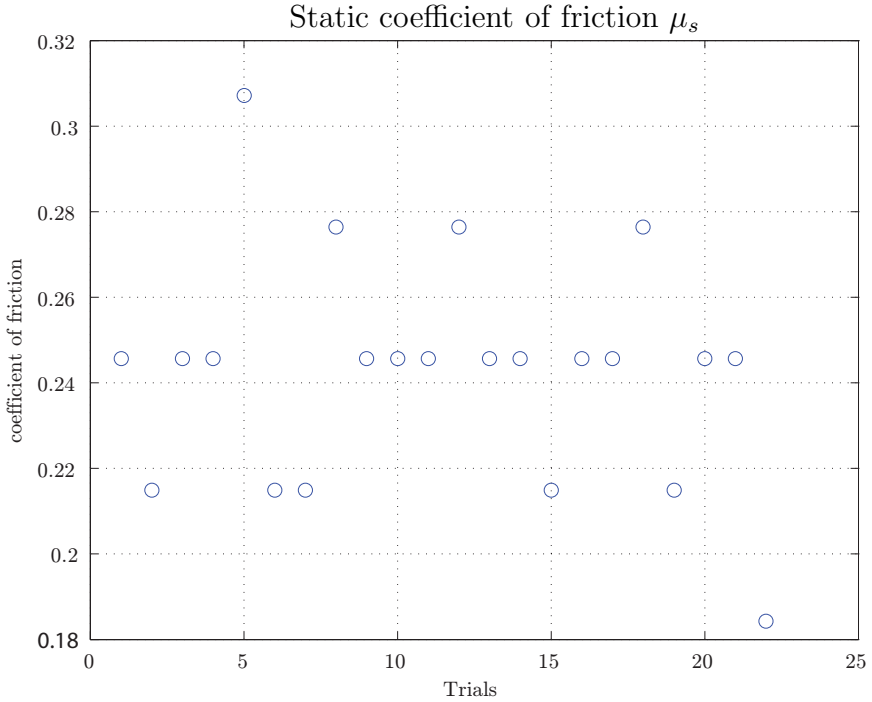

Figure III.5: Static coefficient of friction

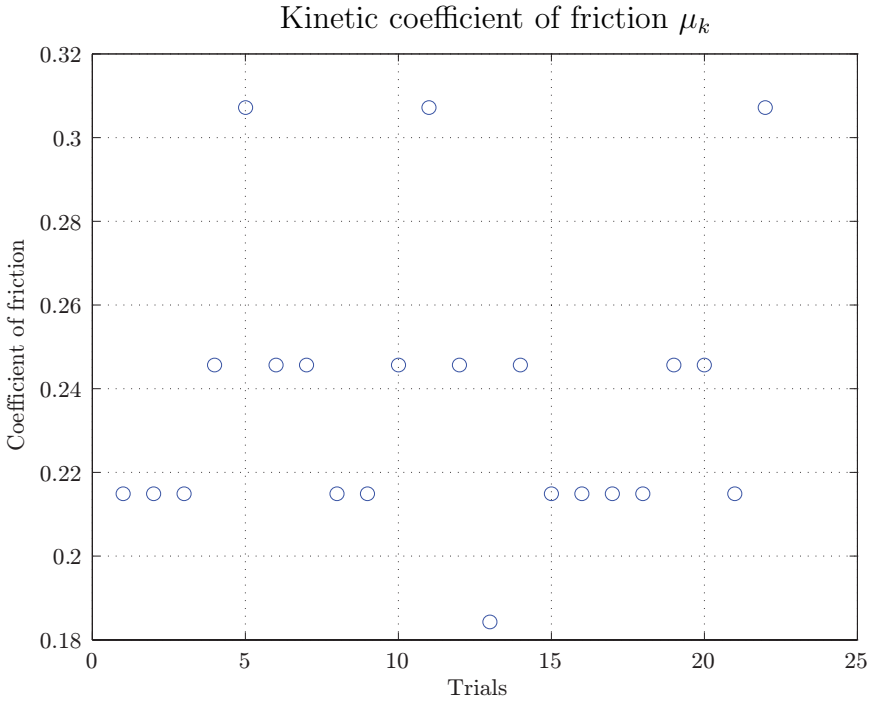

Figure III.6: Kinetic coefficient of friction

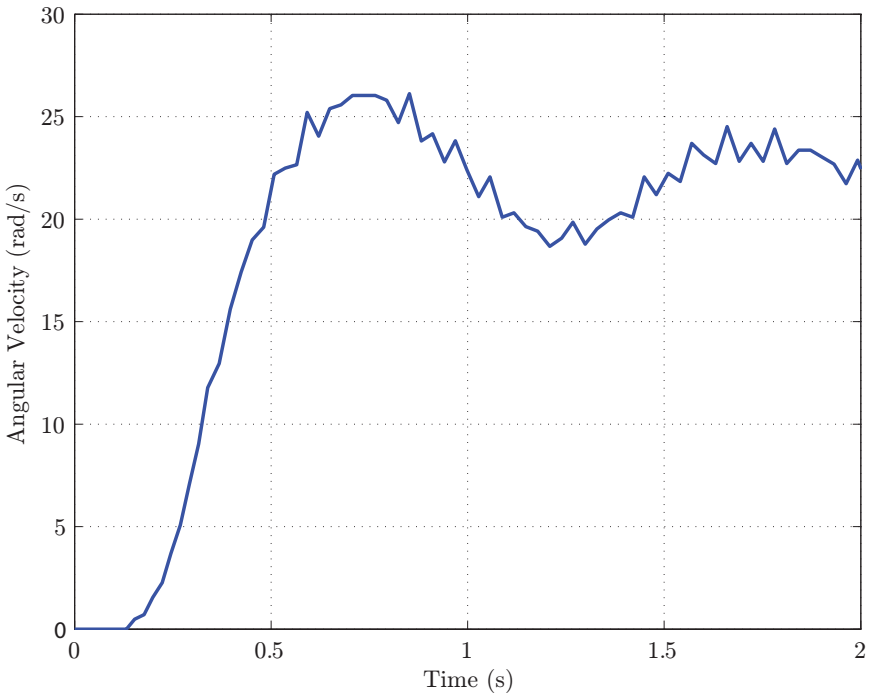

Figure III.7: Measured angular velocity of the wheel at 44 rad/s^2

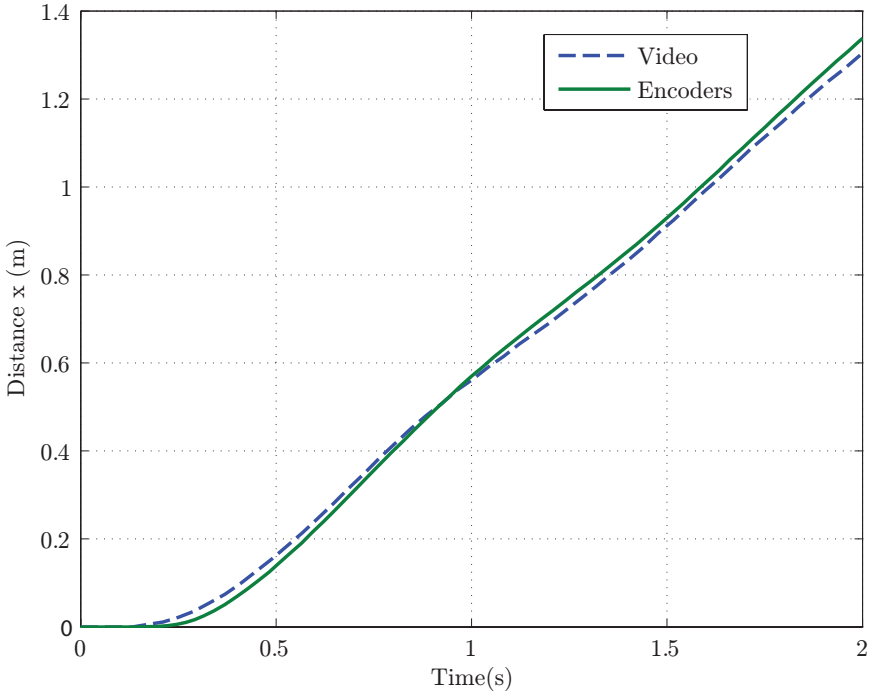

Figure III.8: Measured Robot position at 44 rad/s^2

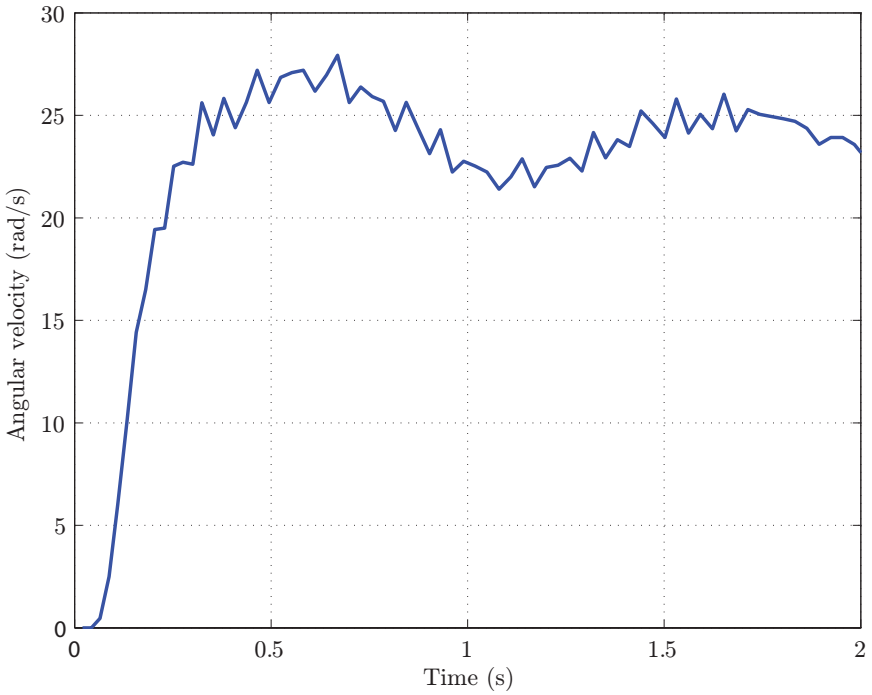

Figure III.9: Measured angular velocity of the wheel at 48 rad/s^2

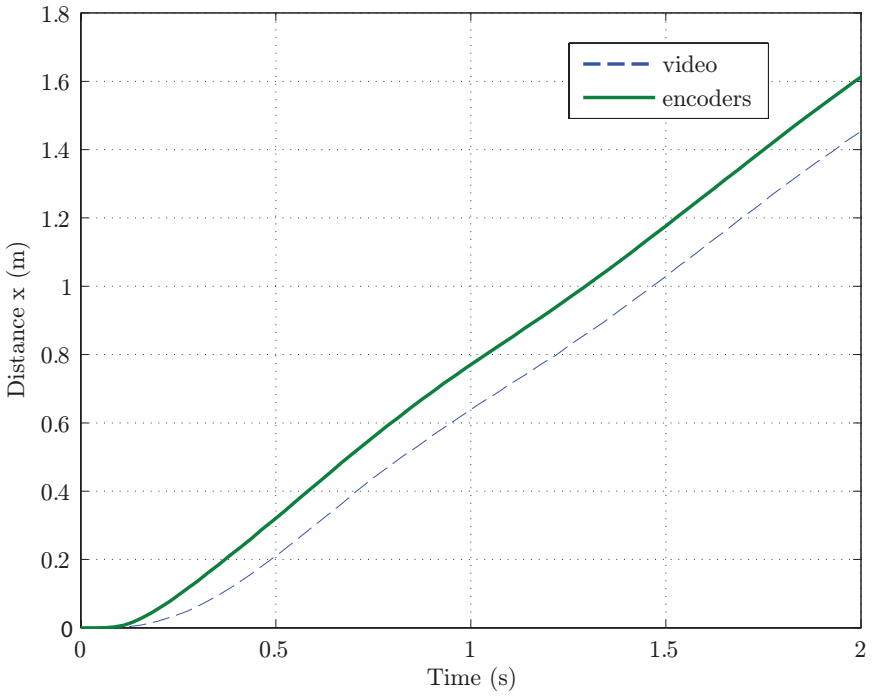

Figure III.10: Measured Robot position at 48 rad/s^2

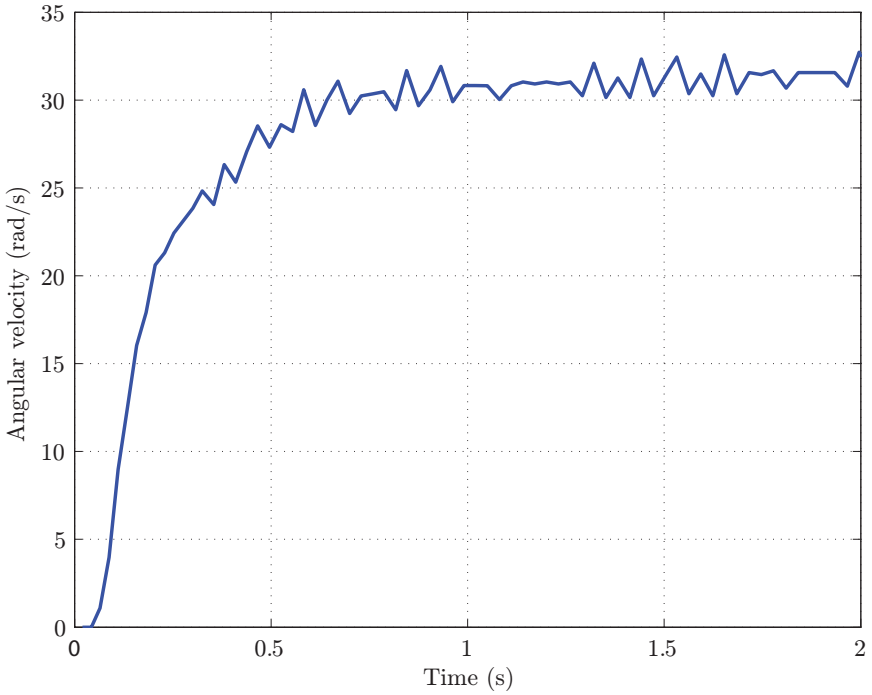

Figure III.11: Measured angular velocity of the wheel at 72 rad/s^2

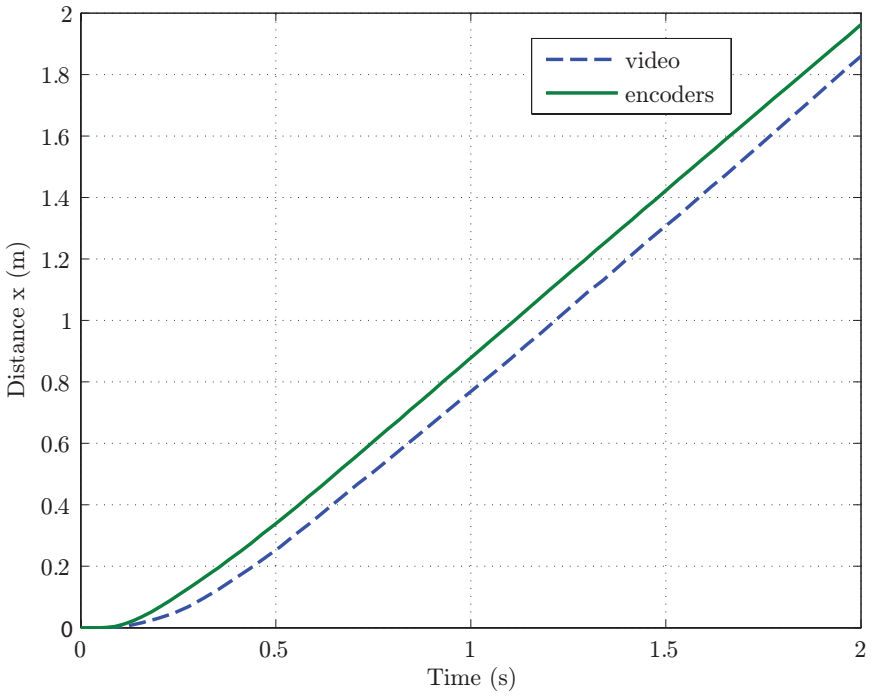

Figure III.12: Measured robot position at 72 rad/s^2

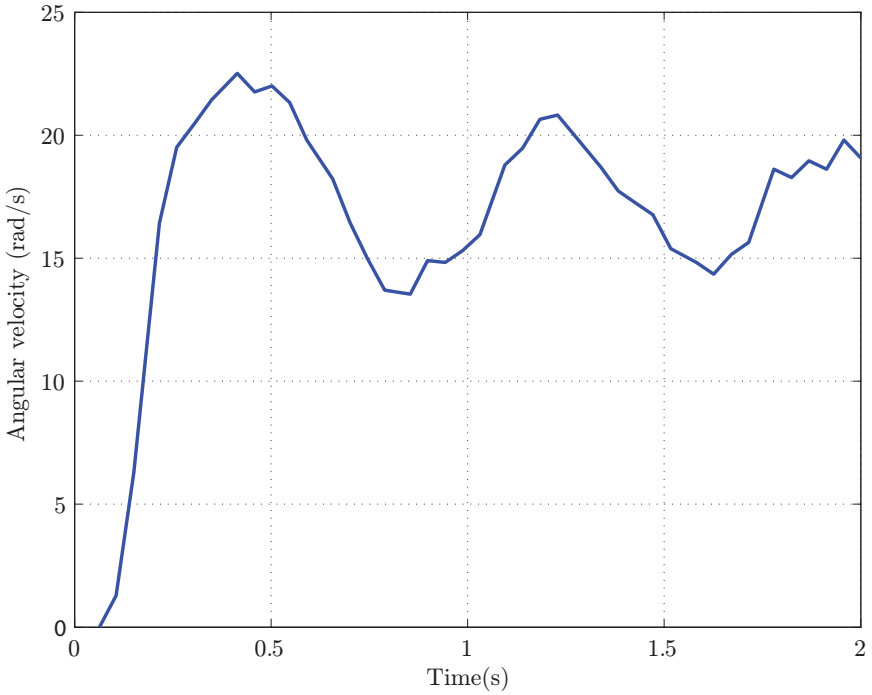

Figure III.13: Measured angular velocity of the wheel at 72 rad/s^2 with torque control

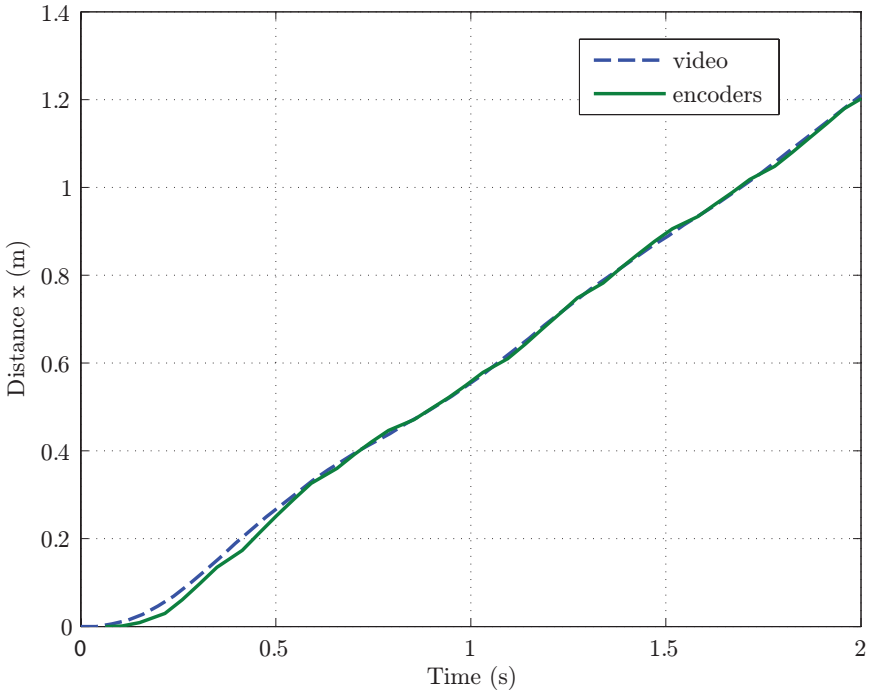

Figure III.14: Measured Robot position at 72 rad/s^2 with torque control

CHAPTER IV

CONCLUSIONS AND FUTURE WORK

Models that describe the dynamics of a differential drive mobile robot with and without slip are presented and discussed. A traction force model was developed by considering a simple Coulomb friction model. From the dynamic analysis it is clear that the caster wheel plays an important role in determining the traction forces, a factor that was not included in the previous work on this subject. A wheel-ground interaction with specific focus on the interaction between rigid wheels and rigid ground is considered to model the traction forces. The longitudinal and lateral velocities of the wheel are used to compute the longitudinal and lateral forces on the wheel instead of the slip velocities.

Wheel slip occurs if the reaction force exerted by the applied torque cannot be completely transmitted to the ground. Therefore, there is a limit to the amount of torque that can be applied to the wheels and the value of this limit depends on the coefficient of static friction. This strategy is used to implement a slip avoidance controller which limits the magnitude of the input torque to a maximum value determined by the proposed traction model.

Simulations of the differential drive dynamics using the proposed traction model reveal the occurrence of slip if the applied torque is greater than the maximum torque that is calculated. Additionally, the effect of slip on angular velocity of the wheels is readily observed which shows that the angular velocity of the wheel is greater than the corresponding linear velocity

when slip occurs. The proposed torque limiting controller to avoid slip was also simulated and it was successful in avoiding slip by limiting the value of the input torques.

Experiments were conducted under the same scenarios as in numerical simulations. The results are comparable which indicates that the robot dynamics model with slip and the traction model describe the dynamics of the differential drive robot. The performance of the torque limiting controller is also verified by experiments.

The following are possible future work topics: (1) The motor dynamics was not included in the simulation models. This may be included in the future to improve the correlation between model simulations and experimental results. (2) In this work the video data was not available for real-time control. If the actual position and velocity of the robot are available in real-time, then feedback controller may be designed to account for slip. (3) Stability characteristics of the torque limiting controller may be further investigated in the future. (4) In this work only straight line trajectories were considered because of actuator and other hardware limitations. One can consider better actuators with non-zero desired robot orientation changes.

REFERENCES

[1] Y. Kanayama, Y. Kimura, F. Miyazaki, and T. Noguchi, "A stable tracking control method for an autonomous mobile robot," in *Proceedings of IEEE International Conference on Robotics and Automation*, pp. 384–389 vol.1, 1990.

[2] X. Yun and Y. Yamamoto, "Internal dynamics of a wheeled mobile robot," in *Proceedings of IEEE/RSJ International Conference on Intelligent Robots and Systems*, vol. 2, pp. 1288–1294 vol.2, 1993.

[3] A. Gholipour and M. Yazdanpanah, "Dynamic tracking control of nonholonomic mobile robot with model reference adaptation for uncertain parameters," in *Proc. of the European Control Conference*, 2003.

[4] P. Petrov, "Modeling and adaptive path control of a differential drive mobile robot," in *Proceedings of the 12th WSEAS international conference on Automatic control, modelling and simulation*, pp. 403–408, 2010.

[5] S. Konduri, "Coordination of multiple autonomous vehicles with directed communication graphs," Master's thesis, Oklahoma State University, 2012.

[6] Y. Zou, *Distributed Control of Multiple Vehicle Systems using Constraint Forces*. PhD thesis, Oklahoma State University, Stillwater, OK, USA, 2008.

[7] "Road test-truck road test and comparisons at gm's milford proving ground." http://trucks.about.com/od/carsafety/ss/truck_safety_5.htm.

[8] "Engine drag torque control." http://www.volkswagen.co.uk/technology/glossary/engine-drag-torque-control.

[9] L. Li, F.-Y. Wang, and Q. Zhou, "Integrated longitudinal and lateral tire/road friction modeling and monitoring for vehicle motion control," *IEEE Transactions on Intelligent Transportation Systems*, vol. 7, no. 1, pp. 1–19, 2006.

[10] R. Balakrishna and A. Ghosal, "Modeling of slip for wheeled mobile robots," *IEEE Transactions on Robotics and Automation*, vol. 11, no. 1, pp. 126–132, 1995.

[11] S. Shekhar, "Wheel rolling constraints and slip in mobile robots," in *Proceedings of IEEE International Conference on Robotics and Automation*, vol. 3, pp. 2601–2607 vol.3, 1997.

[12] K. Yoshida and G. Ishigami, "Steering characteristics of a rigid wheel for exploration on loose soil," in *Proceedings of IEEE/RSJ International Conference on Intelligent Robots and Systems*, vol. 4, pp. 3995–4000 vol.4, 2004.

[13] P. Lamon, A. Krebs, M. Lauria, R. Siegwart, and S. Shooter, "Wheel torque control for a rough terrain rover," in *Proceedings of 2004 IEEE International Conference on Robotics and Automation*, vol. 5, pp. 4682–4687, IEEE, 2004.

[14] A. Angelova, L. Matthies, D. Helmick, G. Sibley, and P. Perona, "Learning to predict slip for ground robots," in *Proceedings of IEEE International Conference on Robotics and Automation*, pp. 3324–3331, 2006.

[15] G. Ishigami, M. Otsuki, T. Kubota, and K. Iagnemma, "Modeling of flexible and rigid wheels for exploration rover on rough terrain," in *Proceedings of the 28th International Symposium on Space Technology and Science*, 2011.

[16] J.-S. Young and B.-J. Wu, "The analysis of the dynamics for the unturned wheels of vehicles," in *The International Conference on Electrical Engineering*, 2008.

[17] S. N. Sidek and N. Sarkar, "Dynamic modeling and control of nonholonomic mobile robot with lateral slip," in *Third International Conference on Systems*, pp. 35–40, 2008.

[18] Y. Tian, N. Sidek, and N. Sarkar, "Modeling and control of a nonholonomic wheeled mobile robot with wheel slip dynamics," in *IEEE Symposium on Computational Intelligence in Control and Automation*, pp. 7–14, 2009.

[19] A. Albagul, Wahyudi, and Wahyudi, "Dynamic modeling and adaptive traction control for mobile robots," in *Proceedings of 30th Annual Conference of IEEE Industrial Electronics Society*, vol. 1, pp. 614–620 Vol. 1, 2004.

[20] S. Nandy, S. Shome, R. Somani, T. Tanmay, G. Chakraborty, and C. Kumar, "Detailed slip dynamics for nonholonomic mobile robotic system," in *International Conference on Mechatronics and Automation*, pp. 519–524, 2011.

[21] S. N. Sidek, *Dynamic Modeling and Control of Nonholonomic Wheeled Mobile Robot Subjected to Wheel Slip*. PhD thesis, Vanderbilt University, 2008.

[22] J. Borenstein and Y. Koren, "Motion control analysis of a mobile robot," *Transactions of ASME, Journal of Dynamics, Measurement and Control*, vol. 109, no. 2, pp. 73–79, 1987.

[23] R. Hibbeler, *Engineering Mechanics: Dynamics*. Prentice Hall PTR, 12th ed., 2010.

[24] "Arduino mega 2560." http://arduino.cc/en/Main/ArduinoBoardMega2560.

[25] "Arduino." http://arduino.cc/en/Main/Software.

[26] "Xbee multipoint rf modules." http://www.digi.com/pdf/ds_xbeemultipointmodules.pdf.

[27] K. Yoshida and G. Ishigami, "Steering characteristics of a rigid wheel for exploration on loose soil," in *Proceedings of IEEE/RSJ International Conference on Intelligent Robots and Systems*, vol. 4, pp. 3995–4000, IEEE, 2004.

[28] "Pentax a ricoh company." http://www.pentax.co.uk/en/digital-slr/specifications/pentax-kr.html.

VITA

Edison Orlando Cobos Torres

Candidate for the Degree of

Master of Science

Thesis: TRACTION MODELING AND CONTROL OF A DIFFERENTIAL DRIVE MOBILE ROBOT TO AVOID WHEEL SLIP

Major Field: Mechanical and Aerospace Engineering

Biographical:

Personal Data: Born in Quito, Pichincha, Ecuador on July 03, 1982.

Education: Received the B.S. degree from Escuela Politécnica Nacional, Quito, Pichincha, Ecuador, 2007, in Mechanical Engineering.
Completed the requirements for the degree of Master Science with a major in Mechanical and Aerospace Engineering in Oklahoma State University, December 2013.

Experience: Assistant Professor at Escuela Politécnica Nacional from September 2009 to August 2011; Graduate Academic Assistant at Escuela Politécnica Nacional, Mechanical Engineering Department from November 2008 to September 2009.
Quality Auditor at Franz Viegener from August 2007 to November 2008; Engineering Coordinator at INCOAYAM from May 2007 to August 2007.

Professional Memberships: Student Member; American Society of Mechanical Engineering; International Society of Automation.